9 The Atmospheric Boundary Layer

by Roland Stull
University of British Columbia, Vancouver, Canada

The Earth's surface is the bottom boundary of the atmosphere. The portion of the atmosphere most affected by that boundary is called the *atmospheric boundary layer* (*ABL*, Fig. 9.1), or *boundary layer* for short. The thickness of the boundary layer is quite variable in space and time. Normally ~1 or 2 km thick (i.e., occupying the bottom 10 to 20% of the troposphere), it can range from tens of meters to 4 km or more.

Turbulence and static stability conspire to sandwich a strong stable layer (called a *capping inversion*) between the boundary layer below and the rest of the troposphere above (called the *free atmosphere*). This stable layer traps turbulence, pollutants, and moisture below it and prevents most of the surface friction from being felt by the free atmosphere.

During fair weather (associated with high-pressure centers), we are accustomed to the diurnal (daily) cycle of changes in temperature, humidity, pollen, and winds that are governed by boundary-layer physics and dynamics. It is cool and calm at night; warm and gusty during daytime. The boundary layer is said to be *unstable* whenever the surface is warmer than the air, such as during a sunny day with light winds over land, or when cold air is advected over a warmer water surface. This boundary layer is in a state of *free convection*, with vigorous thermal updrafts and downdrafts. The boundary layer is said to be *stable* when the surface is colder than the air, such as during a clear night over land, or when warm air is advected over colder water. *Neutral* boundary layers form during windy and overcast conditions, and are in a state of *forced convection*.

Turbulence is ubiquitous within the boundary layer and is responsible for efficiently dispersing the pollutants that accompany modern life. However, the capping inversion traps these pollutants within the boundary layer, causing us to "stew in our own waste." Turbulent communication between the surface and the air is quite rapid, allowing the air to quickly take on characteristics of the underlying surface. In fact, one definition of the boundary layer is that portion of the lower troposphere that feels the effects of the underlying surface within about 30 min or less.

Air masses[1] are boundary layers that form over different surfaces. Temperature differences between neighboring air masses cause baroclinicity that drives extratropical cyclones. Heat and humidity trapped in the boundary layer are important fuels for convective clouds. The capping inversion inhibits thunderstorm formation, allowing the buildup of convective available potential energy (CAPE) in the free atmosphere. Wind shear in the boundary layer, caused by drag near the ground, generates horizontal vorticity that can be tilted by the updrafts in convective clouds to form tornadoes. Dissipation of kinetic energy within the boundary layer serves as a brake on large-scale wind systems.

Turbulence is inspiringly complex, consisting of a superposition of swirls called *eddies* that interact nonlinearly to create quasi-random, chaotic motions. An infinite number of equations is required to fully describe these motions. Hence, a complete solution has not been found. But when averaged over many eddies, we can observe persistent patterns

[1] The term *air mass* refers to an expanse of air with distinctive properties that derive from its residence over a specific source region and are still recognizable for some time after the air has moved into a different geographical setting. For example, air that has resided over a high latitude continent during winter tends to be cold and dry.

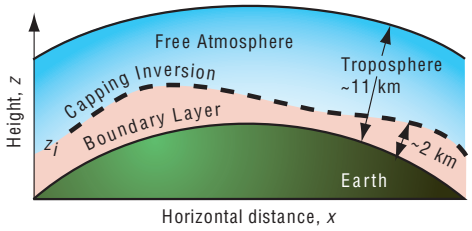

Fig. 9.1 Vertical cross section of the Earth and troposphere showing the atmospheric boundary layer as the lowest portion of the troposphere. [Adapted from *Meteorology for Scientists and Engineers*, A Technical Companion Book to C. Donald Ahrens' Meteorology Today, 2nd Ed., by Stull, p. 65. Copyright 2000. Reprinted with permission of Brooks/Cole, a division of Thomson Learning: www.thomsonrights.com. Fax 800-730-22150.]

and similarities that can be measured and described. In this chapter we explore the fascinating behavior of the boundary layer and the turbulent motions within it.

9.1 Turbulence

Atmospheric flow is a complex superposition of many different horizontal scales of motion (Table 9.1), where the "scale" of a phenomenon describes its typical or average size. The largest are *planetary-scale* circulations that have sizes comparable to the circumference of the Earth. Slightly smaller than planetary scale are *synoptic scale* cyclones, anticyclones, and waves in the jet stream. Medium-size features are called *mesoscale* and include frontal zones, rain bands, the larger thunderstorm and cloud complexes, and various terrain-modulated flows.

Table 9.1 Scales of horizontal motion in the atmosphere

Larger than	Scale	Name
20,000 km		Planetary scale
2,000 km		Synoptic scale
200 km	Meso-α	Mesoscale
20 km	Meso-β	
2 km	Meso-γ	
200 m	Micro-α	Boundary-layer turbulence
20 m	Micro-β	Surface-layer turbulence
2 m	Micro-γ	Inertial subrange turbulence
2 mm	Micro-δ	Fine-scale turbulence
Air molecules	Molecular	Viscous dissipation subrange

Smaller yet are the *microscales*, which contain boundary-layer scales of about 2 km, and the smaller *turbulence* scales contained within it and within clouds. The mesoscale and microscale are further subdivided, as indicated in Table 9.1. This chapter focuses on the microscales, starting with the smaller ones.

9.1.1 Eddies and Thermals

When flows contain irregular swirls of many sizes that are superimposed, the flow is said to be *turbulent*. The swirls are often called *eddies*, but each individual eddy is evanescent and quickly disappears to be replaced by a succession of different eddies. When the flow is smooth, it is said to be *laminar*. Both laminar and turbulent flows can exist at different times and locations in the boundary layer.

Turbulence can be generated *mechanically, thermally*, and *inertially. Mechanical turbulence*, also known as *forced convection*, can form if there is shear in the mean wind. Such shear can be caused by *frictional drag*, which causes slower winds near the ground than aloft; by *wake turbulence*, as the wind swirls behind obstacles such as trees, buildings, and islands (Fig. 9.2); and by *free shear* in regions away from any solid surface (Fig. 9.3).

Thermal or *convective turbulence*, also known as *free convection*, consists of *plumes* or *thermals* of warm air that rises and cold air that sinks due to buoyancy forces. Near the ground, the rising air is often in the form of intersecting curtains or sheets of updrafts, the intersections of which we can identify as *plumes* with diameters about 100 m. Higher in the boundary layer, many such plumes and updraft curtains merge to form larger diameter (~1 km) *thermals*. For air containing sufficient moisture, the tops of these thermals contain cumulus clouds (Fig. 9.4).

Small eddies can also be generated along the edges of larger eddies, a process called the *turbulent cascade*, where some of the *inertial energy* of the larger eddies is lost to the smaller eddies, as eloquently described by Richardson's poem (see Chapter 1). Inertial turbulence is just a special form of shear turbulence, where the shear is generated by larger eddies. The superposition of all scales of eddy motion can be quantified via an *energy spectrum* (Fig. 9.5), which indicates how much of the total turbulence kinetic energy is associated with each eddy scale.

(a)

(b)

Fig. 9.2 Karman vortex streets in (a) the laboratory, for water flowing past a cylinder [From M. Van Dyke, *An Album of Fluid Motion*, Parabolic Press, Stanford, Calif. (1982) p. 56.], and (b) in the atmosphere, for a cumulus-topped boundary layer flowing past an island [NASA MODIS imagery].

Fig. 9.3 Water tank experiments of a jet of water (white) flowing into a tank of clear, still water (black), showing the breakdown of laminar flow into turbulence. [Photograph by Robert Drubka and Hassan Nagib. From M. Van Dyke, *An Album of Fluid Motion*, Parabolic Press, Stanford, CA. (1982), p. 60.]

Turbulence kinetic energy (TKE) is not conserved. It is continually *dissipated* into internal energy by molecular viscosity. This dissipation usually happens at only the smallest size (1 mm diameter) eddies, but

Fig. 9.4 Cumulus clouds fill the tops of (invisible) thermals of warm rising air. [Photograph courtesy of Art Rangno.]

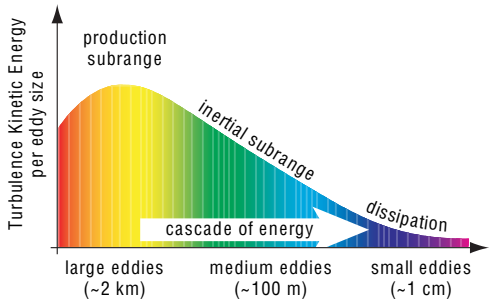

Fig. 9.5 The spectrum of turbulence kinetic energy. By analogy with Fig. 4.2, the total turbulence kinetic energy (TKE) is given by the area under the curve. Production of TKE is at the large scales (analogous to the longer wavelengths in the electromagnetic spectrum, as indicated by the colors). TKE cascades through medium-size eddies to be dissipated by molecular viscosity at the small-eddy scale. [Courtesy of Roland B. Stull.]

it affects all turbulent scales because of the turbulent cascade of energy from larger to smaller scales. For turbulence to exist, there must be continual generation of turbulence from shear or buoyancy (usually into the larger scale eddies) to offset the transfer of kinetic energy down the spectrum of ever-smaller eddy sizes toward eventual dissipation. But why does nature produce turbulence?

Turbulence is a natural response to instabilities in the flow—a response that tends to reduce the instability. This behavior is analogous to *LeChatelier's principle* in chemistry. For example, on a sunny day the warm ground heats the bottom layers of air, making the air statically unstable. The flow reacts to this instability by creating thermal circulations, which move warm air up and cold air down until a new equilibrium is reached. Once this *convective adjustment* has occurred, the flow is statically neutral and turbulence ceases. The reason why turbulence can persist on sunny days is because of continual destabilization by external forcings (i.e., heating of the ground by the sun), which offsets continual stabilization by turbulence.

Similar responses are observed for forced turbulence. Vertical shear in the horizontal wind is a *dynamic instability* that generates turbulence. This turbulence mixes the faster and slower moving air, making the winds more uniform in speed and direction. Once turbulent mixing has reduced the shear, then turbulence ceases. As in the case of convection, persistent mechanical turbulence is possible in the atmosphere only if there is continual destabilization by external forcings, such as by the larger scale weather patterns.

Although the human eye and brain can identify eddies via pattern recognition, the short life span of individual eddies renders them difficult to describe quantitatively. The equations of thermodynamics and dynamics described in Chapters 3 and 7 of this book can be brought to bear on this problem, but the result is an ability to *deterministically* simulate and predict the behavior of each eddy for only exceptionally short durations. The larger diameter thermals can be predicted out to about 15 min to half an hour, but beyond that the predictive skill approaches zero. For smaller eddies of order 100 m, the forecast skill diminishes after only a minute or so. The smallest eddies of order 1 cm to 1 mm can be predicted out to only a few seconds. This inability to deterministically forecast turbulence out to useful periods of days is a result of the highly non-linear nature of turbulent fluid dynamics.

Despite the difficulties of deterministic descriptions of turbulence, scientists have been able to create a *statistical* description of turbulence. The goal of this approach is to describe the net effect of many eddies, rather than the exact behavior of any individual eddy.

9.1.2 Statistical Description of Turbulence

When fast-response velocity and temperature sensors are inserted into turbulent flow, the net effect of the superposition of many eddies of all sizes blowing past the sensor are temperature and velocity signals that appear to fluctuate randomly with time (Fig. 9.6). However, close examination of such a trace reveals that for any half-hour period, there is a well-defined mean temperature and velocity; the range of temperature and velocity fluctuations measured is bounded (i.e., no infinite values); and a statistically robust standard deviation of the signal about the mean can be calculated. That is to say, the turbulence is not completely random; it is *quasi-random*.

Suppose that the velocity components (u, v, w) are sampled at regular time intervals Δt and then digitized and recorded on a computer to form a time series

$$u_i = u\,(i \cdot \Delta t) \tag{9.1}$$

where i is the index of the data point (corresponding to time $t = i\Delta t$) for $i = 1$ to N in a time series of duration $T = N \cdot \Delta t$. The u-component of the *mean wind* $\overline{u}$,

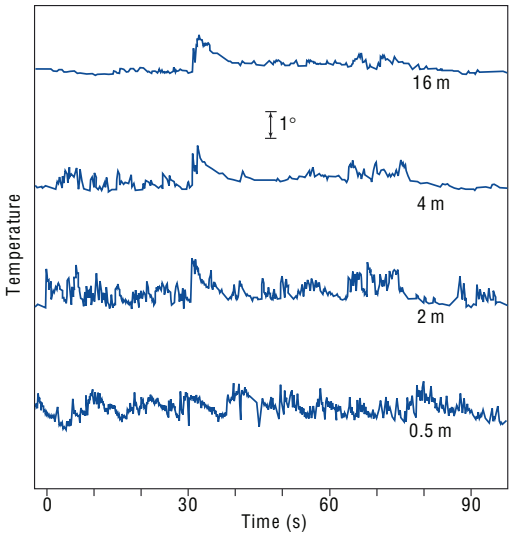

Fig. 9.6 Simultaneous time series of temperature (°C) at four heights above the ground showing the transition from the *surface layer* (bottom 5–10% of the mixed layer) toward the *mixed layer* boundary layer (upper levels of the boundary layer). Observations were taken over flat, plowed ground on a clear day with moderate winds. The top three temperature sensors were aligned in the vertical; the 0.5 m sensor was located 50 m away from the others. [Courtesy of J. E. Tillman.]

based on an average over a time period T (say half an hour), is thus

$$\overline{u} = \frac{1}{N}\sum_{i=1}^{N} u_i \tag{9.2}$$

In the atmosphere, this mean value can change from one half-hour period to the next, resulting in a slow variation of the mean-wind components with time. The velocities referred to in Chapters 7 and 8 are mean velocities (namely, the gusts are averaged out), even though the overbar was not shown. Also, Eq. (9.2) can be generalized: $1/N$ times the sum of N samples of any variable is the average of those samples, and can be indicated by an overbar [e.g., Eq. (9.4)].

Subtracting the mean from the instantaneous component u_i gives just the *fluctuating (gust) portion* of the flow (indicated with a prime)

$$u_i' = u_i - \overline{u} \tag{9.3}$$

which varies rapidly with time. The intensity of turbulence in the u direction is then defined by the *variance*[2]

$$\sigma_u^2 = \frac{1}{N}\sum_{i=1}^{N}[u_i - \overline{u}]^2 = \frac{1}{N}\sum_{i=1}^{N}[u_i']^2 = \overline{[u']^2} \tag{9.4}$$

Again, this is the variance averaged over a half-hour period so this variance value can vary slowly with time over subsequent averaging periods. Similar equations can be defined for the other velocity components.

For situations in which σ_u^2 is relatively constant with time (e.g., the same now as an hour ago), the turbulent nature of the flow is said to be *stationary*. When σ_u^2 is relatively uniform in space (e.g., the same value in one town as in a neighboring town), the flow is said to be *homogeneous*. For situations in which the turbulence intensity at any one point is the same in all directions ($\sigma_u^2 = \sigma_v^2 = \sigma_w^2$), the flow is said to be *isotropic*.

In the atmosphere, fluctuations in velocity are often accompanied by fluctuations in scalar values such as temperature, humidity, or pollutant concentration. For example, in a field of thermals there are regions where warm air is rising (positive potential temperature θ' accompanies positive vertical velocity w'), surrounded by regions where cold air is sinking (negative θ' accompanies negative w'). One measure of the amount that θ and w vary together is the *covariance* (cov)

$$\begin{aligned}\text{cov}\,(w,\theta) &= \frac{1}{N}\sum_{i=1}^{N}[(w_i - \overline{w})\cdot(\theta_i - \overline{\theta})] \\ &= \frac{1}{N}\sum_{i=1}^{N}[(w_i')\cdot(\theta_i')] = \overline{w'\theta'}\end{aligned} \tag{9.5}$$

If warm air parcels are rising and cold parcels are sinking, as in a thermally direct circulation, then $\overline{w'\theta'} > 0$. Covariances can also be negative or zero for different situations in the atmosphere.

The power of the statistical approach is that the velocity variance is more than just a statistic—it represents the *kinetic energy* associated with the motions on the scale of the turbulence. Similarly, the covariance is a measure of *flux* due to these motions, such as the vertical heat flux in Eq. (9.5). Such interpretations are explained next.

9.1.3 Turbulence Kinetic Energy and Turbulence Intensity

Recall from basic physics that kinetic energy is $KE = \frac{1}{2}mV^2$, where m is mass and V is velocity. In meteorology we often use *specific kinetic energy*, namely KE/m, or the kinetic energy per unit mass. By extension, we can focus on just the portion of specific kinetic energy associated with turbulent fluctuations

$$\frac{TKE}{m} = \frac{1}{2}\left[\overline{u'^2} + \overline{v'^2} + \overline{w'^2}\right]$$

or, using (9.4),

$$\frac{TKE}{m} = \frac{1}{2}[\sigma_u^2 + \sigma_v^2 + \sigma_w^2] \tag{9.6}$$

where TKE is *turbulence kinetic energy*. For laminar flow, which contains no microscale motions, $TKE = 0$, even though $\overline{u}$, $\overline{v}$, $\overline{w}$ are not necessarily zero. Larger values of TKE indicate a greater *intensity of the microscale turbulence*. We see now that the three components of velocity variance represent three contributions to the scalar TKE.

[2] Although this is the "biased" variance in statistics terminology, it is negligibly different from the unbiased variance because N is typically very large—~1000 or more. The unbiased variance uses $N - 1$ instead of N in the denominator of Eq. (9.4).

Using what we already know about mechanical and thermal generation of turbulence, and of viscous dissipation, we can write in descriptive form an *Eulerian* (i.e., fixed relative to the ground) forecast equation for turbulence kinetic energy:

$$\frac{\partial(TKE/m)}{\partial t} = Ad + M + B + Tr - \varepsilon \qquad (9.7)$$

where

$$Ad = -\overline{u}\frac{\partial(TKE/m)}{\partial x} - \overline{v}\frac{\partial(TKE/m)}{\partial y} - \overline{w}\frac{\partial(TKE/m)}{\partial z}$$

is the *advection* of *TKE* by the mean wind, *M* is *mechanical generation* of turbulence, *B* is *buoyant generation or consumption* of turbulence, *Tr* is *transport* of turbulence energy by turbulence itself, and ε is the viscous *dissipation rate*. The terms *Ad* and *Tr* neither create nor destroy *TKE*, they just *redistribute* it by moving it from one location to another. *M* is usually positive (or zero if there is no shear) and therefore *generates* turbulence, while *B* can be positive or negative. Dissipation is always negative and can be approximated by $\varepsilon = (TKE/m)^{3/2}/L_\varepsilon$, where L_ε is a *dissipation length scale*.

In the absence of the terms *Ad, M, B*, and *Tr*, we see that as long as *TKE* is nonzero, the last term will always cause *TKE* to decrease toward zero. For this reason, turbulence is said to be *dissipative*.

In statically stable environments the buoyancy term can reduce *TKE* by converting it to potential energy by moving cold air up and warm air down. In such situations, the existence of turbulence depends on the relative strengths of mechanical generation (*M*) by wind shear versus buoyant consumption (*B*) by static stability. The ratio of these two terms defines the dimensionless *Richardson number, Ri*, which can be approximated by the vertical gradients of wind and potential temperature

$$Ri = \frac{-B}{M} = \frac{\dfrac{g}{\overline{T}_v}\dfrac{\partial\overline{\theta}_v}{\partial z}}{\left(\dfrac{\partial\overline{u}}{\partial z}\right)^2 + \left(\dfrac{\partial\overline{v}}{\partial z}\right)^2} \qquad (9.8)$$

where the term in the numerator is equivalent to the square of the Brunt Väisälä frequency, as defined in (3.75). Laminar flow becomes turbulent when *Ri* drops below the critical value $Ri_c = 0.25$. Turbulent flow often stays turbulent, even for Richardson numbers as large as 1.0, but becomes laminar at larger values of *Ri*. The presence or absence of turbulence for $0.25 < Ri < 1.0$ depends on the history of the flow: a behavior analogous to hysteresis. Flows for which $Ri_c < 0.25$ are said to be *dynamically unstable*.

When the shear in laminar flow across a density interface (e.g., between cold air below and warm air above) increases to the point at which the flow becomes dynamically unstable, the turbulence onset grows as a *Kelvin-Helmholtz (KH) instability* on the interface. First, small waves appear that grow in amplitude and curl over on themselves. If sufficient moisture is present in the atmosphere, a cloud can form in the rising portions of each curl, giving rise to a pattern that looks like breaking waves at the beach when viewed from the side (Fig. 9.7a). When viewed from above or below, these features appear as closely spaced parallel bands of clouds, called *KH billows* or *billow clouds* (Fig. 9.7b), which are perpendicular to the vertical shear vector $\partial\mathbf{V}/\partial z$. The overturning of the billows introduces static instabilities (i.e., locally unstable lapse rates) that further accelerate the transition to turbulence within the shear layer.

The shapes of turbulent eddies are also modulated by the static stability. Under statically unstable conditions with rising thermals, the largest eddies are strongly *anisotropic*, with much greater turbulent energy in the vertical motion component than in the horizontal component. For continuous emissions of smoke from a smoke stack, smoke plumes *loop* up and down and spread more rapidly in the vertical than in the horizontal. Under statically neutral conditions, turbulence is almost isotropic, and smoke plumes spread equally in the vertical and in the horizontal, yielding a conical envelope, a behavior referred to as *coning*. When the flow is statically stable but dynamically unstable, the vertical component of turbulence is partly suppressed by the negative buoyancy of the rising air and the positive buoyancy of the sinking air—a process referred to as *buoyant consumption*—resulting in anisotropy with moderate TKE in the horizontal motion component but very little energy in the vertical component. Smoke plumes in such an environment *fan* out horizontally. In extremely stable conditions, turbulence is completely suppressed, and smoke blows downwind with almost no dispersion, although the plume centerline can oscillate up and down as a laminar wave.

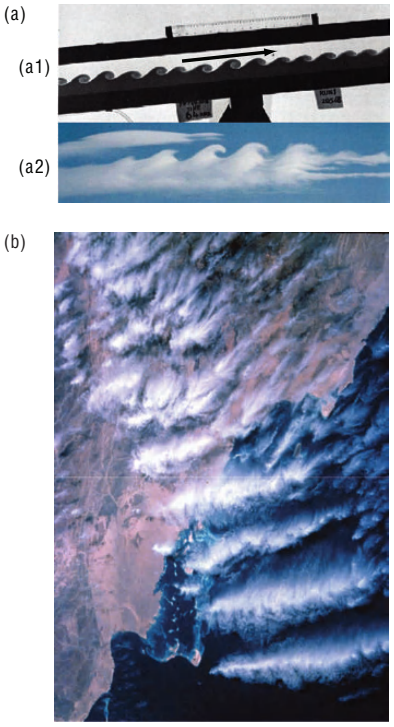

Fig. 9.7 (a) Kelvin–Helmholtz waves (b) Kelvin–Helmholtz billows in clouds. Kelvin–Helmholtz (KH) breakdown of shear flow. (a1) A long narrow water tank is filled with a layer of salt brine (dyed a dark color) in the bottom half and clear, fresh water in the top half. When the tank is tilted, the heavy brine flows downslope (to the left in this photo) and the lighter fresh water flows upslope, creating a shear across the density interface. [From *J. Fluid Mech.*, 46 (1971) p. 299, plate 3.] (a2) Similar breaking of KH waves at an atmospheric density interface, by chance made visible by clouds. [Courtesy of Brooks Martner.] (b) KH billow clouds in the atmosphere as viewed from above. [NASA MODIS imagery.]

9.1.4 Turbulent Transport and Fluxes

Covariances can be interpreted as fluxes using the following concepts. Consider a portion of the atmosphere with a constant gradient of potential temperature, as sketched in Fig. 9.8. Consider an idealized eddy circulation consisting of an updraft portion that moves an air parcel from the bottom to the top of the layer, and a compensating downdraft that moves a different air parcel downward. Air mass is conserved (i.e., mass up = mass down). However, the air parcels carry with them small portions of the air from their starting points, and these portions preserve their potential temperatures as they move, resulting in a flux as will now be shown.

In Fig. 9.8a, the thick line represents a statically unstable mean environment $[\bar{\theta}(z)]$. For this case when the rising air parcel reaches its destination, its potential temperature is warmer than the surrounding environment at that altitude. Namely, its deviation from its new environment is $\theta' = (+)$. This air parcel had to move upward to get to its destination so $w' = (+)$. The contribution of this rising parcel to the total covariance is w' times $\theta' = w'\theta' = (+) \cdot (+) = (+)$. Similarly, for the downward-moving $[w' = (-)]$ portion of this eddy, the cold air from aloft finds itself colder $[\theta' = (-)]$ than its new surrounding environment at its final low altitude. Thus, its contribution to the covariance is $w'\theta' = (-) \cdot (-) = (+)$.

The average of these two air parcels represents the covariance, and since each contribution is positive, the average (indicated by the overbar) is also positive: $\overline{w'\theta'} = (+)$. Thus, positive $\overline{w'\theta'}$ covariance is associated with warm air moving up and/or cold air moving down, namely a positive *heat flux* $F_H(=\overline{w'\theta'})$. This form of flux is called a *kinematic heat flux* and has units of (K m s^{-1}). It is related to the traditional heat flux Q_H (W m^{-2}) by

$$Q_H = \rho c_p F_H = \rho c_p \overline{w'\theta'} \tag{9.9}$$

where ρ is the mean air density and c_p is the specific heat of air at constant pressure.

Figure 9.8b shows the contrasting behavior observed in a statically stable environment. In this case, both the upward and downward moving parcels contribute negatively to the covariance. Thus, a downward heat flux is associated with cold air moving up or warm air moving down. Hence, the covariance $F_H = \overline{w'\theta'}$ is negative.

These fluxes can contribute to the warming and cooling of layers of air via the first law of thermodynamics (see Chapter 3), which, in the absence of other heat sources, can be rewritten as

$$\frac{\partial \bar{\theta}}{\partial t} = -\frac{\partial \overline{w'\theta'}}{\partial z} + \cdots \tag{9.10}$$

Note also the analogy with radiative fluxes in the expression for radiative heating rates (4.52).

The net result of this turbulence is that warmer and colder layers are mixed to yield an intermediate potential temperature. In a similar manner, one can

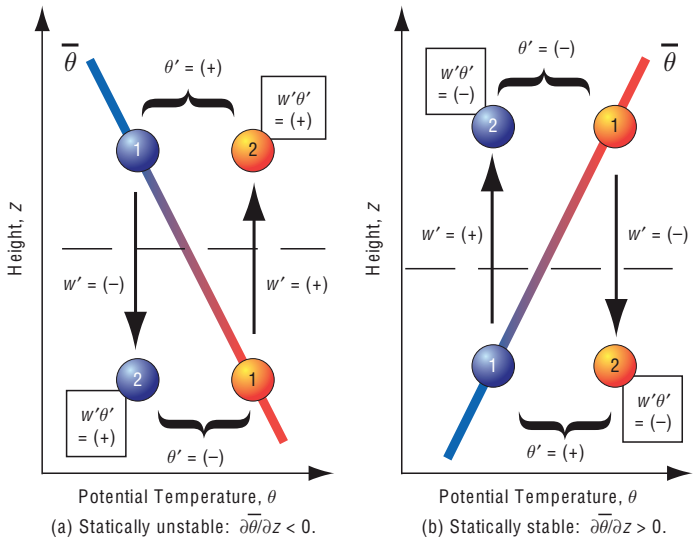

Fig. 9.8 Illustration of how to anticipate the sign of turbulent heat fluxes for small-eddy (local) vertical mixing across a region with a linear gradient in the mean potential temperature θ (thick colored line). Assuming an adiabatic process (no mixing), air parcels (sketched as spheres) preserve their potential temperature (as indicated by their color) of the ambient environment at their starting points (1), even as they arrive at their destinations (2). (a) Statically unstable lapse rate. (b) Statically stable lapse rate. [Adapted from *Meteorology for Scientists and Engineers*, A Technical Companion Book to C. Donald Ahrens' Meteorology Today, 2nd Ed., by Stull, p. 87. Copyright 2000. Reprinted with permission of Brooks/Cole, a division of Thomson Learning: www.thomsonrights.com Fax 800-730-2215.]

conceive of turbulent mixing of moisture, pollutants, and even momentum. In each case, turbulence tends to *homogenize* a fluid.

Turbulence is an extremely efficient mixer. For example, when milk is added to coffee or tea, most people prefer not to wait hours for molecular diffusion to homogenize their drink. Instead, they stir the fluid to generate turbulence, which homogenizes their drink within a few seconds. Atmospheric turbulence is equally efficient at causing mixing—so much so that molecular diffusion and molecular viscosity can be neglected for all motions except the tiniest eddies. In fact, during the daytime over land, convective turbulence is so effective at mixing that the boundary layer is also known as the *mixed layer* because pollutants are distributed so quickly in the vertical.

9.1.5 Turbulence Closure

Equation (9.10) is a forecast equation for potential temperature. The overbar on all the terms in this equation is associated with a process called *Reynolds averaging*—an applied mathematical method that eliminates small *linear* terms such as those associated with nonbreaking *waves*, but retains the *non-linear* terms associated with, or affected by, *turbulence*. There are many other terms that appear on the right-hand side of the full Reynolds-averaged forecast equation, but for now we will focus on just the heat-flux divergence term. To forecast how the mean potential temperature will change with time, we need to know the kinematic heat flux $\overline{w'\theta'}$.

A Reynolds-averaged forecast equation can also be derived for kinematic heat flux $\overline{w'\theta'}$, which is of the form

$$\frac{\partial \overline{w'\theta'}}{\partial t} = -\frac{\partial \overline{w'w'\theta'}}{\partial z} + \cdots \qquad (9.11)$$

This new equation yields a forecast of the second-order statistic $\overline{w'\theta'}$, but it introduces a new third-order statistic $\overline{w'w'\theta'}$, which is the turbulent flux of a heat flux. If we write a forecast equation for this third-order statistic, we introduce even higher order unknowns.

This is the *turbulence closure problem*. Mathematically speaking, the equations are not closed. There are always more unknowns than equations. In other words, we need an infinite number of equations to describe turbulence, even if we want only to forecast the mean potential temperature.

To mitigate this difficulty, we can make *closure assumptions*. Namely, we can retain a finite number of equations and then approximate the remaining unknowns as a function of the knowns. The resulting *parameterization* will not give a perfect answer, but it will give an approximate answer that often is good enough.

Turbulence closure assumptions are categorized both by their *statistical order* and by the amount of *nonlocalness* that is included. For the statistical order, if we keep Eq. (9.10) and approximate the unknown $\overline{w'\theta'}$ as a function of the known variables, the result is called *first-order closure*, named after the highest order forecast equation retained. Second-order closure retains both Eqs. (9.10) and (9.11) and parameterizes the third-order statistics $\overline{w'w'\theta'}$.

A common local, first-order closure is called *gradient-transfer theory, K-theory, eddy-diffusivity theory*, or *mixing-length theory*. Analogous to molecular diffusion, it assumes that the flux is linearly proportional to and directed down the local gradient, i.e.,

$$F_H = \overline{w'\theta'} = -K\frac{\partial\bar{\theta}}{dz} \tag{9.12}$$

where an eddy diffusivity, K, is used instead of the molecular diffusivity. The parameter K is prescribed to increase with the intensity of the turbulence, which varies with height above ground, mean wind shear, and surface heating by the sun. Prandtl's[3] mixing length approach was one of the first parameterizations for eddy diffusivity: $K = l^2|\partial V/\partial z|$, where V is mean horizontal wind speed and $l = \left(\overline{z'^2}\right)^{1/2}$ represents an average size or *mixing length* for the eddies. The parameter l is often approximated by $l = k\,z$ in the *surface layer* (the bottom 5 to 10% of the boundary layer), where $k = 0.4$ is the von Karman[4] constant and z is height above ground level. The wind-shear term in K parameterizes the effects of mechanical generation of turbulence.

The closure in Eq. (9.12) is a *local closure* in the sense that the heat flux at any altitude depends on the local gradient of potential temperature at that same altitude. Namely, it implicitly assumes that only small-size eddies exist. Similar first-order closures can be written for moisture, pollutant, and momentum fluxes.

While local first-order closures often work nicely in laboratory settings, they frequently fail in the unstable atmospheric boundary layer. Under these conditions, thermals cause such intense mixing and homogenization as to eliminate the vertical gradient of mean potential temperature in the middle of the boundary layer, yet there are strong positive heat fluxes caused by the rising thermals. For this situation, *nonlocal* first-order closures have been developed, where the flux across any one altitude depends on transport by all eddy sizes, including the large eddies that move heated air from just above the Earth's surface all the way to the top of the boundary layer.

Finally, a large body of useful results have been complied for statistical *zeroth-order closure*. In this case, neither Eqs. (9.10) nor (9.11) is retained. Instead, the mean flow state $\bar{\theta}$ is parameterized directly. This approach, called *similarity theory*, is illustrated in the next subsection.

9.1.6 Turbulence Scales and Similarity Theory

Some zero and first-order closure schemes rely on simple empirical[5] relationships derived from *dimensional analysis*. Variables that frequently appear in combination with one another are grouped to form new variables that may be nondimensional, such as the Richardson number defined in Eq. (9.8), or may have simple dimensional units such as velocity, length, or time that in some cases relate to the most important scales of motion in the eddies.

A velocity scale that is useful for characterizing the turbulent mixing due to free convection in an

[3] **Ludwig Prandtl** (1874–1953) German aerodynamicist and accomplished pianist. Developed theories for the boundary layer, airfoils, lift vs. drag, and supersonic flow for rocket nozzles. Educated in Munich in mechanics, became professor in Hannover, and later directed the Institute for Technical Physics and the Kaiser Wilhelm Institute for Flow Investigation, University of Göttingen, Germany.

[4] **Theodor von Kármán** (1881–1963) Hungarian aerodynamicist, specializing in supersonic flight. Studied boundary layers and airfoils under Ludwig Prandtl and became professor of aeronautics and mechanics at the University of Aachen, Germany. Worked with Hugo Junkers to help design the first cantilevered wing all metal airplane in 1915. Became director of the Guggenheim Aeronautical Lab at the California Institute of Technology, advancing theoretical aerodynamics and rocket design, and spawning the Jet Propulsion Lab. Was the first recipient of the U.S. National Medal of Science, awarded by John F. Kennedy.

[5] Based on observed relationships between variables.

unstably stratified boundary layer is the *Deardorff velocity scale*

$$w_* = \left[\frac{g \cdot z_i}{T_v}\overline{w'\theta'_s}\right]^{1/3} \tag{9.13}$$

where z_i is the depth of the boundary layer and the subscript s denotes at the surface. Values of w_* have been determined from field measurements and numerical simulations under a wide range of conditions. Typical magnitudes of w_* are $\sim 1\ \mathrm{m\ s^{-1}}$, which corresponds to the average updraft velocities of thermals.

Another scale u_*, the *friction velocity*, is most applicable to statically neutral conditions in the surface layer, within which the turbulence is mostly mechanically generated. It is given by

$$u_* = \left[\overline{u'w'}^2 + \overline{v'w'}^2\right]^{1/4} = \left|\frac{\tau_s}{\rho}\right|^{1/2} \tag{9.14}$$

where ρ is air density, τ_s is *stress* at the surface (i.e., drag force per unit surface area), and covariances $\overline{u'w'}$ and $\overline{v'w'}$ are the *kinematic momentum fluxes* (vertical fluxes of u and v horizontal momentum, respectively).

The altitude of the capping inversion, z_i, is the relevant length scale for the whole boundary layer for statically unstable and neutral conditions. Within the bottom 5% of the boundary layer (referred to as the *surface layer*), an important length scale is the *aerodynamic roughness length*, z_0, which indicates the roughness of the surface (see Table 9.2). For statically nonneutral conditions in the surface layer, there is an additional length scale, called the *Obukhov length*

$$L \equiv \frac{-u_*^3}{k \cdot (g/T_v) \cdot \left(\overline{w'\theta'}\right)_s}, \tag{9.15}$$

where $k = 0.4$ is the von Karman constant. The absolute value of L is the height below which mechanically generated turbulence dominates.

Typical timescales for the convective boundary layer and the neutral surface layer are

$$t_* = \frac{z_i}{w_*} \qquad t_{*SL} = \frac{z}{u_*} \tag{9.16}$$

where z is height above the surface.
For the convective boundary layer, t_* is of order 15 min, which corresponds to the turnover time for the largest convective eddy circulations, which extend from the Earth's surface all the way up to the capping inversion.

In summary, for convective boundary layers (i.e., unstable mixed layers), the relevant scaling parameters are w_* and z_i. For the neutral surface layer, u_* and z_0 are applicable. Scaling parameters for surface

Table 9.2 The Davenport classification, where z_o is aerodynamic roughness length and C_{DN} is the corresponding drag coefficient for neutral static stability[a]

z_0 (m)	Classification	Landscape	C_{DN}
0.0002	Sea	Calm sea, paved areas, snow-covered flat plain, tide flat, smooth desert.	0.0014
0.005	Smooth	Beaches, pack ice, morass, snow-covered fields.	0.0028
0.03	Open	Grass prairie or farm fields, tundra, airports, heather.	0.0047
0.1	Roughly open	Cultivated area with low crops and occasional obstacles (single bushes).	0.0075
0.25	Rough	High crops, crops of varied height, scattered obstacles such as trees or hedgerows, vineyards.	0.012
0.5	Very rough	Mixed farm fields and forest clumps, orchards, scattered buildings.	0.018
1.0	Closed	Regular coverage with large size obstacles with open spaces roughly equal to obstacle heights, suburban houses, villages, mature forests.	0.030
≥2	Chaotic	Centers of large towns and cities, irregular forests with scattered clearings.	0.062

[a] From Preprints *12th Amer. Meteorol. Soc. Symposium on Applied Climatology*, 2000, pp. 96–99.

layers are u_*, z_0, and L, provided that the stratification is not neutral.

As an example, when dimensional analysis is used to describe the vertical profile of the variance of vertical velocity $\overline{w'^2}$ through the entire depth of the convective boundary layer, the observational data are fit by the function

$$\frac{\overline{w'^2}}{w_*^2} = a\left(\frac{z}{z_i}\right)^b\left(1 - c\frac{z}{z_i}\right)^d$$

in which a, b, c, and d are constants. This expression for dimensionless velocity variance as a function of dimensionless height is applicable to convective boundary layers of any depth and for any surface heat flux. That is to say, vertical profiles of $\overline{w'^2}$ exhibit similar shapes and collapse onto a single curve when plotted on the same pair of dimensionless coordinate axes ($\overline{w'^2}/w_*^2$ versus z/z_i): hence the name *similarity theory*.

When applied to observational data for the statically stable surface layer, dimensional analysis yields the vertical profile of horizontal wind speed

$$\frac{V}{u_*} = 2.5\ln\left(\frac{z}{z_0} + 8.1\frac{z}{L}\right)$$

This expresson for dimensionless speed as a function of dimensionless height is applicable for any wind speed, height, roughness, and static stability in the surface layer (i.e., the vertical profiles exhibit similar shapes and collapse onto a single similarity curve).

As we have seen, the nature of turbulence is strongly modulated by heat fluxes and drag (momentum fluxes) at the surface. The next section describes the daily evolution of these surface fluxes under fair weather (anticyclonic) conditions.

Exercise 9.1 (a) What is the relationship between the Obukhov length and the Deardorff velocity? (b) For a 1-km-thick boundary layer with a surface kinematic heat flux of 0.2 K m s^{-1} and surface kinematic stress of 0.2 m^2 s^{-2}, over what portion of the boundary layer does mechanical turbulence dominate?

Solution: (a) Combining Eqs. (9.13) and (9.15) yields

$$L/z_i = -u_*^3/(k{\cdot}w_*^3)$$

(b) $u_*^3 = (0.2\ \text{m}^2\ \text{s}^{-2})^{3/2} = 0.089\ \text{m}^3\ \text{s}^{-3}$. Assuming $T_v = 300$ K as a typical value, then $w_*^3 = 6.5\ \text{m}^3\ \text{s}^{-3}$. Thus, $|L/z_i| = 0.089/(0.4)\ (6.5) = 0.034$. The mechanically driven surface layer is only 3.4% of the convective boundary layer depth for this example. It is often the case that the surface layer is much thinner than 10% of the boundary-layer depth under free-convective conditions. ■

9.2 The Surface Energy Balance

9.2.1 Radiative Fluxes

The solar radiation incident on the Earth's surface is modulated by the rotation of the Earth, causing a daily (*diurnal*) cycle of incoming solar radiation with reference to local sunrise, noon, and sunset over any point on the surface.

Let $F_s\downarrow$ be the magnitude of the flux of downwelling solar (shortwave) radiation that reaches the surface, integrated over all wavelengths in and near the visible spectrum. The surface reflects some of the sunlight back upward, of magnitude $F_s\uparrow$. Also, the atmosphere emits longwave radiation, some of which $F_L\downarrow$ reaches the Earth's surface. The Earth's surface emits longwave radiation upward, with flux magnitude $F_L\uparrow$. The sum of the inputs to the surface minus the outputs yields the *net radiation flux* F^* absorbed at the surface

$$F^* = F_s\downarrow - F_s\uparrow + F_L\downarrow - F_L\uparrow \qquad (9.17)$$

During fair weather with clear skies, the surface radiation fluxes vary with time as sketched in Fig. 9.9. During daytime, the incoming solar radiation is proportional to the sine of the elevation angle of the sun, which varies with time of day, latitude, and season. The solar radiation reflected from the Earth's surface mirrors the incoming direct solar radiation, but with reduced amplitude. At night, there is obviously no shortwave radiation.

The upward and downward longwave fluxes nearly cancel. The $F_L\uparrow$ curve has a slight modulation, which reflects the changing skin temperature [via the Stefan-Boltzmann law (4.12)] of the Earth's surface as it warms and cools in response to variations in solar radiation. Because of their small heat capacity, land surfaces respond almost instantaneously: thus, $F_L\uparrow$ is virtually in phase with the $F_s\downarrow$ flux. However, the $F_L\downarrow$ curve depends on the air temperature, which reaches its maximum in late afternoon before sunset and reaches its minimum just after sunrise.

The algebraic sum of all these fluxes, F^*, is nearly constant and slightly negative during the night and

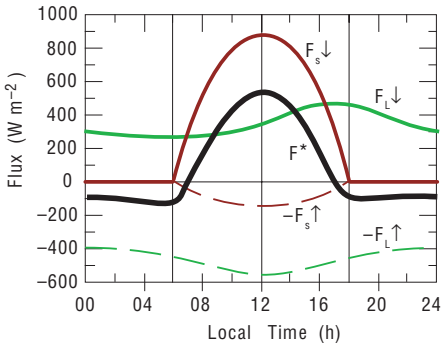

Fig. 9.9 Sketch of contribution of radiative fluxes at the Earth's surface toward the net flux F^* during a daily cycle under clear skies. Positive values represent inputs toward the surface; negative are fluxes away. [Adapted from *Meteorology for Scientists and Engineers,* A Technical Companion Book to C. Donald Ahrens' Meteorology Today, 2nd Ed., by Stull, p. 37. Copyright 2000. Reprinted with permission of Brooks/Cole, a division of Thomson Learning: www.thomsonrights.com. Fax 800-730-2215.]

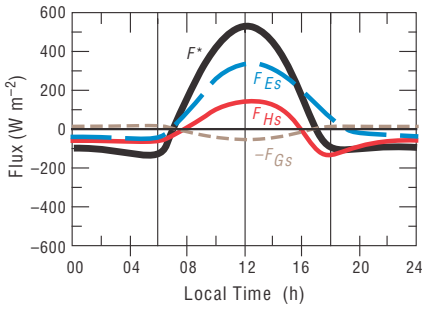

Fig. 9.10 Sketch of the disposition of the net flux F^* into turbulent sensible F_H and latent F_E heat fluxes into the atmosphere at the surface (subscript s), and conduction of heat into the ground F_G during a daily cycle under clear skies. Except for F^* (which is the same as in Fig. 9.9), positive displacements from zero along the ordinate represent upward fluxes, and negative downward. [Adapted from *Meteorology for Scientists and Engineers,* A Technical Companion Book to C. Donald Ahrens' Meteorology Today, 2nd Ed., by Stull, p. 57. Copyright 2000. Reprinted with permission of Brooks/Cole, a division of Thomson Learning: www.thomsonrights.com. Fax 800-730-2215.]

becomes positive with peak near solar noon during daytime, where the sign is defined such that positive implies an input to the surface. This is the "*external*" *forcing* that drives the diurnal variations in the surface heat budget.

9.2.2 Surface Energy Balance over Land

In addition to the radiative fluxes at the Earth's surface, the fluxes of sensible and latent heat also need to be taken into account. The sensible heat flux heats the air in the boundary layer directly. The latent heat flux (i.e., the flux of water vapor times L, the latent heat of vaporization) is not converted to sensible heat and/or potential energy until the water vapor condenses in clouds.

If we imagine the land surface as an infinitesimally thin surface that has zero heat capacity, then the heat flux coming in must balance the heat leaving. Given the net radiation F^* from the previous section, Fig. 9.10 shows how energy gain or loss is partitioned among *sensible heat flux,* F_{Hs}, into the air (positive upward, for flux away from the surface), *latent heat flux* F_{Es} into the air (positive upward), and the *conduction* of heat down into the ground, F_{Gs} (positive downward, away from the surface), where the extra subscript s denotes near the surface. Therefore,

$$F^* = F_{Hs} + F_{Es} + F_{Gs} \qquad (9.18)$$

In fair weather conditions with light to calm winds, Fig. 9.11 shows the direction of the fluxes during day and night. Over moist lawns, crops, and forests, most of the sun's energy goes into evaporation during daytime. However, during daytime over a dry desert or unvegetated land (Fig. 9.11c), most of the sun's energy goes into sensible heat flux.

During windy conditions if dry, hot air is advected over a cool, moist surface, such as at a desert oasis (Fig. 9.11d), then the sensible heat flux can be downward from the warm air to the cool surface, even though there is also solar heating of the surface. These two inputs combine to create very large evaporation and associated latent heat flux, known as the *oasis effect*. As a basis for understanding why the surface has this response over desert oases, the next subsection explains bulk aerodynamic methods for estimating surface fluxes.

The magnitude of flux into the ground, F_{Gs}, is ~10% of the net radiation magnitude during daytime, increasing to ~50% at night. The amplitude of the diurnal cycle of surface skin temperature, T_s, is inversely proportional to the conductivity of the soil. The annual cycle of soil temperature as a function of depth, shown in Fig. 9.12, is qualitatively similar to its counterpart for the diurnal cycle (not shown), but it penetrates to a greater depth. Amplitude decreases with increasing depth and the phase becomes progressively later. Bearing in mind that heat is always conducted down

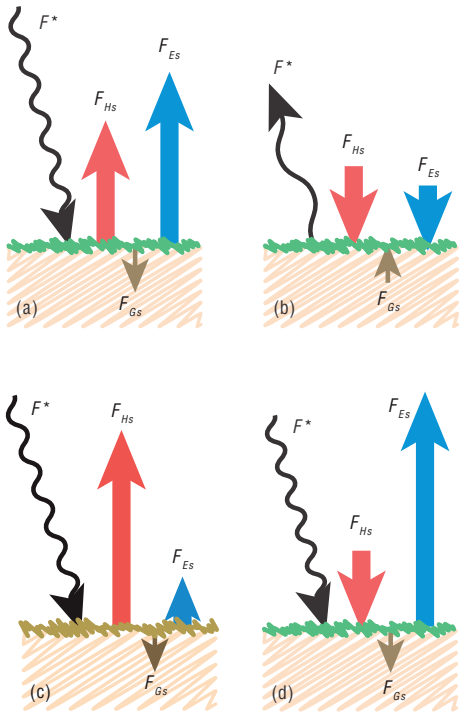

Fig. 9.11 Vertical cross-section sketch of net radiative input to the surface flux, F^*, and resulting heat fluxes into the air and ground for different scenarios (a) Daytime over a moist vegetated surface. (b) Nighttime over a moist vegetated surface. (c) Daytime over a dry desert. (d) Oasis effect during the daytime, with hot dry wind blowing over a moist vegetated surface. (See Fig. 9.10 for explanation of symbols.) [Adapted from *Meteorology for Scientists and Engineers*, A Technical Companion Book to C. Donald Ahrens' Meteorology Today, 2nd Ed., by Stull, p. 57. Copyright 2000. Reprinted with permission of Brooks/Cole, a division of Thomson Learning: www.thomsonrights.com. Fax 800-730-2215.]

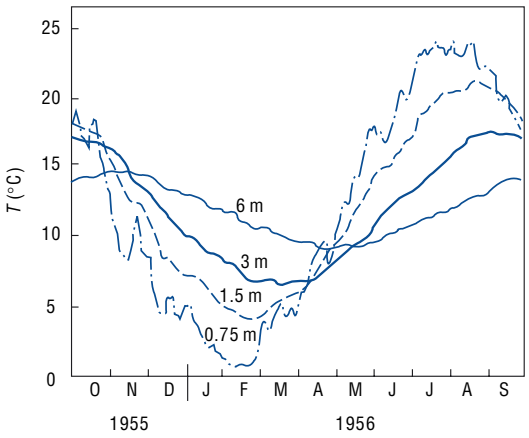

Fig. 9.12 Soil temperatures recorded at an exposed site at levels below the ground. [Adapted from *Trans. Amer. Geophys. Union* 37, 746 (1956).]

the gradient from higher temperature toward lower temperature, it is evident that the downward conduction of heat reduces the warming of the land surface during periods of strong heat input, when the soil temperature decreases with depth, while the upward conduction of heat from below reduces the cooling of the surface during periods of weak insolation.

Ocean surfaces exhibit much larger values of F_{Gs} because turbulence in the ocean can quickly mix heat throughout the top layer of the ocean, called the *ocean mixed layer*, which ranges in depth from a few meters to hundreds of meters. The specific heat of liquid water is also larger than that of soil. These two effects conspire to give the ocean a much larger heat capacity than the land surface, enabling it to absorb and store solar energy during the day and release it at night, resulting in nearly constant ocean surface temperatures through the diurnal cycle, and allowing only small temperature changes through the annual cycle.

9.2.3 The Bulk Aerodynamic Formulae

This subsection describes a method that can be used to estimate the fluxes of sensible and latent heat at the Earth's surface. This so-called *bulk aerodynamic method* enables us to estimate the frictional drag on the surface winds as well.

Sensible heat flux between the surface and the overlying air is driven by two processes. Within the bottom few millimeters of the atmosphere, very large vertical gradients of temperature form, causing *molecular conduction* of heat away from the surface into the air. At the bottom of this molecular layer (e.g., at the surface of the ground), there is zero turbulent flux because clods of soil do not usually "dance the eddy dance." But from the top of this *molecular layer* or *microlayer* to the top of the boundary layer, molecular conduction is negligible while *turbulent convection* takes over, moving the warm air upward to distribute sensible heat throughout the boundary layer. Because the microlayer is so thin compared to the boundary-layer depth and because the heat flux across the microlayer is nearly constant and equal to the turbulent eddy flux at the top of the microlayer, it is possible to define an *effective turbulent flux* that is the sum of the molecular and true turbulent components. In practice, the word

"effective" is often omitted, and this quantity is referred to simply as the *turbulent flux at the surface*.

The effective sensible heat flux is often parameterized by the temperature difference between the surface and the air. If the surface skin temperature, T_s, is known, then the sensible heat flux (in kinematic units of K m s^{-1}) from the ground to the air can be parameterized as

$$F_{Hs} = C_H |V| (T_s - T_{air}) \qquad (9.19a)$$

where C_H is a dimensionless *bulk transfer coefficient* for heat and $|V|$ and T_{air} are the wind speed and air temperature at standard surface measurement heights (10 and 2 m, respectively). To convert from kinematic to dynamic heat flux (W m^{-2}), F_H must be multiplied by air density times the specific heat at constant pressure ($\rho\, c_p$).

Under statically neutral conditions over flat land surfaces there exists a moderate amount of turbulence that exchanges slow moving air near the ground with faster moving air in the boundary layer, yielding values for C_H in the 0.001 – 0.005 range (designated as C_{H_N} to indicate neutral conditions). The exact value of C_{H_N} depends on surface roughness, similar to the roughness dependence of C_{D_N} shown in Table 9.2.

Under statically unstable conditions, the vigorous turbulence communicates surface drag information more quickly to the boundary layer, causing C_H to be two to three times as large as C_{H_N}. Conversely, as the air becomes more statically stable, the Richardson number increases toward its critical value and the turbulence kinetic energy decreases toward zero, causing C_H to also decrease toward zero.

To estimate the vertical heat flux, one might have expected Eq. (9.19a) to be function of a vertical turbulent-transport velocity w_T times the temperature difference. But for this first-order closure, w_T is parameterized as $C_H|V|$, where it is assumed that stronger winds near the ground generate stronger turbulence, which causes stronger turbulent fluxes.

By combining Eqs. (9.17–9.19a), we see that the surface skin temperature over land on sunny days is really a response to solar heating rather than an independent driving force for the heat flux. For example, on a day with light winds, the net radiation budget causes a certain energy input to the ground, which causes the surface skin temperature to rise according to the first law of thermodynamics. As the skin warms, the sensible heat flux increases in accordance with Eq. (9.19a), as does the evaporation and the conduction of heat into the ground. Since the winds are light, (9.19a) shows that the skin temperature must become quite a bit warmer than the air temperature to drive sufficient sensible heat flux F_{Hs} to help balance the surface heat budget. However, on a windier day, the required heat flux is achieved with a surface skin temperature that is only slightly warmer than the air temperature.

When warmer air is advected over a cooler surface or when the ground is cooled by longwave radiation at night, then $T_s < T_{air}$, and the heat flux becomes downward. This cools the bottom of the boundary layer, and leads to *sub-adiabatic lapse rates* and a reduction or suppression of turbulence. Because turbulence is reduced, the cooling is limited to the bottom of the boundary layer, creating a shallow *stable boundary layer* embedded within the old, deeper boundary layer.

Similar equations, called *bulk aerodynamic relationships*, can be derived for the moisture flux over oceans, lakes, and saturated soil. One can assume that the specific humidity near the surface q_s is equal to its saturation value, as defined by the Clausius-Clapeyron equation, based on the air temperature near the sea surface. Namely, the moisture flux F_{water} [in kinematic units of ($kg_{water\ vapor}/kg_{air}$) (m s^{-1})] from the surface is

$$F_{water} = C_E |V| [q_{sat}(T_s) - q_{air}] \qquad (9.19b)$$

where C_E is a dimensionless bulk transfer coefficient for moisture ($C_E \approx C_H$). This moisture flux is directly related to the latent heat flux (F_{Es}, in kinematic units of K m s^{-1}) at the surface and to the evaporation rate E of water (mm/day) by

$$F_{water} = \gamma F_{Es} = (\rho_{liq}/\rho_{air})\, E \qquad (9.20)$$

where $\gamma = c_p/L_v = 0.4$ [($g_{water\ vapor}/kg_{air}$)/K] is the *psychometric constant* and ρ_{liq} is the density of pure liquid water (not sea water).

The ratio of sensible to latent heat fluxes at the surface is called the *Bowen ratio*[6]: $B = F_{Hs}/F_{Es}$. Due to

[6] **Ira S. "Ike" Bowen** (1898–1973) American physicist and astronomer. Studied under Robert A. Millikan as a graduate student at the University of Chicago and as a research assistant at the California Institute of Technology, where his Ph.D. was on evaporation from lakes and associated heat losses. Identified ultraviolet spectral lines from nebulae. Directed Mt. Wilson and Palomar observatories and the construction of the Hale and Schmidt telescopes. Worked with the Jet Propulsion Laboratory on photography from rockets.

the nonlinearity inherent in the Clausius-Clapeyron equation, the Bowen ratio over the oceans decreases with increasing sea surface temperature. Typical values range from around 1.0 ± 0.5 along the ice edge to less than 0.1 over the tropical oceans where latent heat fluxes dominate due to the warmth of the sea surface. Over land, the evaporation rate, and therefore the Bowen ratio, depends on the availability of water in the soil and on the makeup of the vegetation that transports water from the soil via osmosis. Plants release water vapor into the air via *transpiration* through the open stomata (pores) of leaves. Thus, the Bowen ratio ranges from about 0.1 over tropical oceans, through 0.2 over irrigated crops, 0.5 over grassland, 5.0 over semiarid regions, and 10 over deserts.

For momentum, the bulk aerodynamic approach gives a *drag law*

$$u_*^2 = C_D |V|^2 \tag{9.19c}$$

where C_D is the dimensionless *drag coefficient*, ranging in magnitude from 10^{-3} over smooth surfaces to 2×10^{-2} over rough ones (Table 9.2), and u_*^2 is the magnitude of momentum flux lost downward into the ground. C_D is affected not only by *skin friction* (viscous drag), but also by *form drag* (pressure gradients upwind and downwind of obstacles such as trees, buildings, and mountains) and by *mountain-wave drag*. Hence, C_D can be larger than C_H. The drag coefficient C_D varies with stability relative to its neutral value CD_N in the same manner as C_H; namely, C_D CD_N for unstable boundary layers, and C_D CD_N for stable boundary layers.

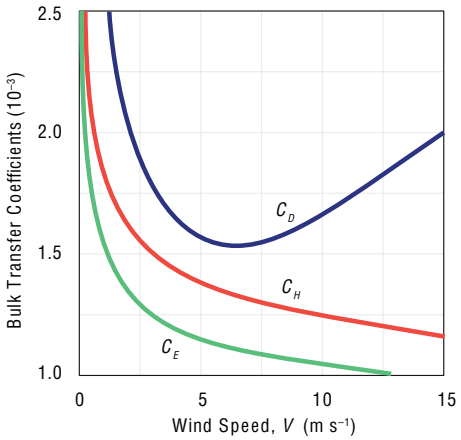

Fig. 9.13 Variation of bulk transfer coefficients for drag (C_D), heat (C_H), and moisture (C_E) with wind speed over the ocean. [Adapted from an unpublished manuscript by M. A. Bourassa and J. Wu (1996).]

Over oceans, an increase in the wind speed leads to an increase in the wave height, which also increases the drag (see Box 9.1). Figure 9.13 shows how the bulk transfer coefficients for momentum, heat, and humidity vary with wind speed measured at height $z = 10$ m over the oceans. For wind speeds larger than 5 m s^{-1}, heat and moisture transfer coefficients gradually decrease with increasing wind speed, whereas the drag coefficient C_D increases. For wind speeds much less than 5 m s^{-1} the bulk formulae are inapplicable, because the vertical turbulent transport between the surface and the air depends more on convective thermals than on wind speed.

9.1 Winds and Sea State

A surface wind gust passing over a water surface produces a discernible patch of tiny *capillary waves* with crests aligned perpendicular to the surface wind vector. Since capillary waves are short lived, their distribution at any given time reflects the current distribution of surface wind. Remote sensing of capillary waves by satellite-borne instruments, called *scatterometers*, provides a basis for monitoring surface winds over the oceans on a global basis.

When forced by surface winds over periods ranging from hours to days, waves with different wavelengths and orientations interact with each other to produce a continuous spectrum of ocean waves extending out to wavelengths of hundreds of meters. The stronger and more sustained the winds, the larger the amplitude of the longer wavelengths. *Wind waves* with the shorter wavelengths tend to propagate in the same direction as the winds. In contrast, the faster propagating long wavelengths tend to radiate outward from regions of strong winds to become *swells* and may thus provide the first sign of an approaching storm. The incidence of wave breaking increases with wind speed. At speeds in excess of 50 m s^{-1}, wave breaking becomes so intense and extensive that the air-sea interface becomes diffuse and difficult to define.

Chapter 7 showed how winds can be forecast by considering the sum of all forces acting on the air. Turbulent drag, as just discussed, is one such force, which always acts opposite to the wind direction (i.e., it slows the wind). More importantly, we see from (9.19c) that the strength of the drag force is proportional to the square of the wind speed, so doubling the wind speed quadruples the drag.

Through these fluxes at the bottom of the atmosphere, the characteristics of the underlying surface are impressed upon the air within the atmospheric boundary layer, but not upon the air in the overlying free atmosphere. Over land the diurnal variations in these fluxes are spread by turbulence throughout the depth of the boundary layer, causing diurnally varying vertical profiles, as described in the next section.

Exercise 9.2 Consider a column of air initially of vertically uniform θ over cold land, capped by a very strong temperature inversion that prevents boundary layer growth. This air column advects with speed U over a warmer ocean surface with potential temperature θ_s. (a) How does temperature vary with distance x from shore? (b) At any fixed distance x from shore, how does the air temperature vary with wind speed?

[**Hint**: Use Taylor's[7] hypothesis: $\dfrac{\partial\theta}{\partial t} = U\dfrac{\partial\theta}{\partial x}$.]

Solution: If the only heat into the air column is from the surface, then the change of air temperature with time is found from the heat budget Eq. (9.10) integrated over the boundary layer depth: $\partial\theta/\partial t = F_{Hs}/z_i$, where z_i is constant. Combining this with Taylor's hypothesis gives

$$\frac{\partial\theta}{\partial x} = \frac{1}{U}\frac{F_{Hs}}{z_i}$$

Then, estimating the surface heat flux with bulk aerodynamic methods (Eq. 9.19a) and approximating $(T_s - T)$ by $(\theta_s - \theta)$ gives

$$\frac{\partial\theta}{\partial x} = C_H\frac{\theta_s - \theta}{z_i}$$

(a) Separate variables and integrate: $\theta = \theta_s - (\theta_s - \theta_0)\exp[-C_H x/z_i]$, where θ_0 is the initial potential temperature of the air over land. Thus, the air temperature increases with downwind distance x from the shoreline, rapidly at first, but more gradually further downstream as the air temperature asymptotically approaches the sea-surface temperature.

(b) Surprisingly, air temperature at a fixed distance from shore is independent of wind speed. The reason is that while faster winds cause larger heat fluxes and faster warming of the boundary layer, the faster wind also reduces the time available for warming before the air reaches any distance x from shore. ■

9.2.4 The Global Surface Energy Balance

By applying the bulk aerodynamic formulae to global data sets in which fields of surface air temperature, sea- and land surface temperature, incident solar radiation, and downwelling longwave radiation are derived from assimilation of in situ and space-based observations into state-of-the-art numerical weather prediction models, it is possible to estimate the global distribution of the various terms in the surface energy balance. The net upward transfer of energy through the Earth's surface is

$$F_{net}^{\uparrow} = -F^* + F_{Hs} + F_{Es} \qquad (9.21)$$

where F^* is the net downward radiative flux. The sum of the three terms on the right-hand side of (9.21) may be recognized as being equivalent to the term F_{Gs} in (9.18).

The geographical distribution of the annual mean $F_{net}^{\uparrow}$ is shown in Fig. 9.14. As in the net radiation balance at the top of the atmosphere discussed in Section 4.6, the global mean of $F_{net}^{\uparrow}$, averaged over the year, is very close to zero. However, there are local imbalances in excess of 100 W m^{-2}. Because of the small heat capacity of the land surfaces, the net fluxes over the continents are small. The largest imbalances are over regions of the oceans in which the sea

[7] **Geoffrey Ingram Taylor** (1886–1975) British mathematician, physicist, and meteorologist. Studied shock waves, quantum theory, and atmospheric turbulence. Served as meteorologist on an iceberg patrol ship, deployed after ocean liner Titanic collided with an iceberg and sank. Lectured on dynamical meteorology at Cambridge University, devised a statistical method to study turbulent dispersion, examined deformation of crystals, and studied fluid dynamics. Enjoyed boating and flying.

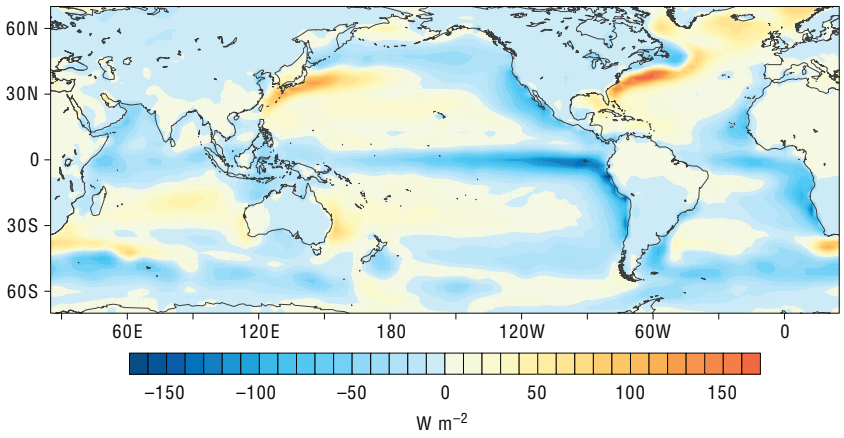

Fig. 9.14 Annual-mean net upward energy flux at the Earth's surface as estimated from Eq. (9.21) based on a reanalysis of 1958–2001 data by the European Centre for Medium Range Weather Forecasting. [Courtesy of Todd P. Mitchell.]

surface is anomalously warm or cold relative to the mean temperature at that latitude (Fig. 2.11). The net flux is upward over the warm waters of the Gulf Stream and the Kuroshio current and it is downward over the regions of coastal and equatorial upwelling where cold water is being brought to the surface.

9.3 Vertical Structure

This section considers the interplay between turbulence and the vertical profiles of wind, temperature and moisture within the boundary layer, drawing heavily on the diurnal cycle over land as an example.

9.3.1 Temperature

Depending on the vertical temperature structure within the boundary layer, turbulent mixing can be suppressed or enhanced at different heights via buoyant consumption or production of T. In fact, it is ultimately the temperature profile that determines the boundary-layer depth.

Recall that the troposphere is statically stable on average, with a potential temperature gradient of 3.3 °C/km (Fig. 9.15). Solar heating of the ground causes thermals to rise from the surface, generating turbulence. Also, drag at the ground causes near-surface winds to be slower than winds aloft, creating wind shear that generates mechanical turbulence. Turbulence generated by processes near the ground mixes surface air of relatively low values of potential temperature, with higher potential temperature air

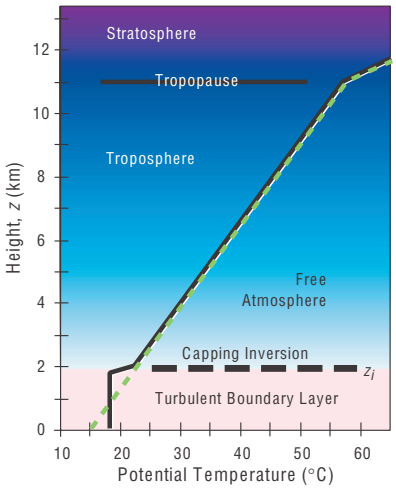

Fig. 9.15 Standard atmosphere (dashed line) in the troposphere and lower stratosphere, and its alteration by turbulent mixing in the boundary layer (solid line). [Adapted from *Meteorology for Scientists and Engineers*, A Technical Companion Book to C. Donald Ahrens' Meteorology Today, 2nd Ed., by Stull, p. 67. Copyrigt 2000. Reprinted with permission of Brooks/Cole, a division of Thomson Learning: www.thomsonrights.com. Fax 800-730-2215.]

from higher altitudes. The resulting mixture has an intermediate potential temperature that is relatively uniform with height (i.e., homogenized within the boundary layer). More importantly, this low altitude mixing has created a temperature jump between the boundary-layer air and the warmer air aloft. This temperature jump corresponds to the capping inversion.

The capping inversion is characterized by high static stability, which suppresses turbulence within it. Turbulence from below has difficulty penetrating the capping inversion and is thus confined within the boundary layer. Hence, the net result is a feedback: boundary-layer turbulence helps create the capping inversion, and the capping inversion tends to trap the turbulence in the boundary layer.

Compared to the mid- and upper troposphere, the fair-weather boundary layer over land exhibits a much larger temperature response to the diurnal cycle because of the rapid turbulent transport forced by alternating heating and cooling of the underlying surface. This effect appears in upper-air soundings as rapid diurnal changes of the vertical profiles within the boundary layer, with slower synoptic scale changes aloft in the free atmosphere. Figure 9.16 contrasts typical vertical profiles of potential temperature and other variables in the boundary layer over land, for day and night. During the daytime, the θ profile is nearly uniform with height over most of the middle of the boundary layer. Because of this extreme homogenization, the daytime boundary layer is also known as the mixed layer, as previously mentioned. Near the bottom is a surface layer (roughly 5% of the depth of the mixed layer), with a superadiabatic temperature gradient, as required to cause a positive heat flux into the air. Near the top is the statically stable capping inversion, which during the daytime is called the *entrainment zone*. Above that is the free atmosphere, illustrated here with the statically stable *standard atmosphere*.

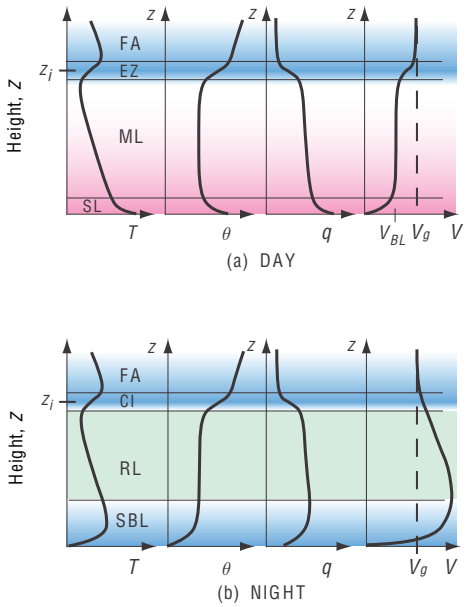

Fig. 9.16 Sketch of typical vertical profiles of temperature (T), potential temperature (θ), specific humidity (q), and wind speed (V) in the bottom of the troposphere. FA, free atmosphere; EZ, entrainment zone; ML, mixed layer; SL, surface layer; CI, capping inversion; RL, residual layer; SBL, stable boundary layer; z_i, height of the capping inversion, which equals top of the boundary layer (BL); V_g, geostrophic wind speed. [Adapted from *Meteorology for Scientists and Engineers*, A Technical Companion Book to C. Donald Ahrens' Meteorology Today, 2nd Ed., by Stull, p. 70. Copyright 2000. Reprinted with permission of Brooks/Cole, a division of Thomson Learning: www.thomsonrights.com. Fax 800-730-2215.]

As mentioned previously, a second stable layer (called the *stable boundary layer* or the *nocturnal boundary layer*) forms at night near the ground in response to the cooling of the air by the radiatively cooled surface. Aloft, the capping inversion formed the previous day is still present. The stable boundary layer near the ground consumes *TKE*, resulting in weak and sporadic turbulence there. Between these two stable layers is the *residual layer*, which contains dying or zero turbulence and also the residual heat, moisture, and pollutants that were mixed there during the previous day.

9.3.2 Humidity

Figure 9.16 also shows the profile of specific humidity, q. During fair weather, the free atmosphere is relatively dry because of the subsiding air in anticyclones (i.e., highs). Evaporation from the surface during daytime adds moisture to the boundary layer. The net result is that there is a rapid decrease of specific humidity with height in the surface layer, as expected by the bulk aerodynamic formula to drive moisture fluxes from the ground into the boundary layer. The moisture added from the ground causes the mixed layer to be more humid than the free-atmosphere air aloft and leads to a humidity jump across the capping inversion.

At night, humidities in most of the middle and top of the boundary layer do not change due to turbulence because turbulence has diminished. However, the radiatively cooled surface can cause dew or frost formation, which reduces humidity in the very bottom of the boundary layer. On other occasions, when dew or frost do not occur, the specific humidity is relatively uniform throughout the bottom and middle of the boundary layer.

9.3.3 Winds

Drag at the ground always causes the wind speed to be reduced, while aloft the winds are stronger (Fig. 9.16). In general, wind speed in the surface layer exhibits a nearly logarithmic profile, as approximated by

$$\overline{V} = \frac{u_*}{k} \ln\left(\frac{z}{z_0}\right) \tag{9.22}$$

where $k = 0.4$ is the von Karman constant and z_0 is the *aerodynamic roughness length* (Table 9.2). The roughness length is defined as the height of zero wind speed as extrapolated down logarithmically from the stronger winds in the surface layer.

Exercise 9.3 By analogy with (9.12) it is possible to define an *eddy viscosity coefficient*

$$K \equiv \frac{-\overline{w'u'}}{\partial \overline{U}/\partial z}$$

that relates the intensity of the vertical mixing of zonal momentum to the local vertical gradient of zonal wind speed, and similarily for the meridional wind component. As in the first-order turbulence closure scheme discussed in Section 9.1.6, K is a local measure of the intensity of the turbulent eddies that are responsible for mixing horizontal momentum downward through the surface layer to the Earth's surface. (a) What is the relationship between eddy viscosity K and height z that yields the logarithmic wind profile (9.22), and what does this suggest about surface-layer similarity theory? (b) What is the relationship between roughness length and drag coefficient? [**Hints**: Let the horizontal mean winds be $(\overline{U}, 0)$ and consider Reynolds stress in only the x-direction.]

Solution: (a) Use Eq. (9.22) for the logarithmic wind profile and assume total wind speed = $\overline{U}$,

$$\overline{U} = (u_*/k)\, ln(z/z_0) = (u_*/k)\,[\ln(z) - \ln(z_0)]$$

Take the partial derivative with respect to height z

$$\partial \overline{U}/\partial z = u_*/(kz)$$

Substituting

$$u_*^2 = -\overline{w'u'} = K\frac{\partial \overline{U}}{\partial z}$$

and solving for K we obtain

$$K = k\, z\, u_*$$

It follows that K must increase linearly with height in the surface layer to yield a logarithmic wind profile. K increases with u_*, the square root of the wind stress at the surface, consistent with the notion that windier conditions should be marked by stronger turbulence, which leads to more vigorous eddy mixing. Finally, since the logarithmic wind profile is consistent with a K-theory approach, the fact that it is observed implies that the dominant form of turbulence in the surface layer is small-eddy mixing (i.e., local mixing).

(b) Combine Eq. (9.19c) with the logarithmic wind profile equation

$$C_D = [k/\ln(z/z_0)]^2$$

Thus, rougher surfaces (large z_0) are associated with larger values of the drag coefficient C_D for statically neutral conditions. ■

Equation (9.22) is an example of zeroth-order turbulence closure. It is based on the similarity theory that all wind profiles under statically neutral conditions collapse to one common logarithmic curve (i.e., the curves look similar to each other) when the dimensionless wind speed V/u_* is plotted versus the dimensionless height z/z_0. Often, the expression for wind in the surface layer is written in terms of a dimensionless wind shear

$$\Phi_M = \frac{kz}{u_*}\frac{\partial V}{\partial z} \tag{9.23}$$

where $k = 0.4$ is the von Karmam constant. Thus, for statically neutral conditions, the vertical derivative of Eq. (9.22) can be written as

$$\Phi_M = 1 \tag{9.24}$$

The wind-profile shape varies slightly with static stability, but in general is logarithmic in the surface layer (Fig. 9.17). Under statically stable conditions that are still turbulent (i.e., when $z/L > 0$), the profile is well described by the empirical relationship

$$\Phi_M = 1 + 8.1\frac{z}{L} \tag{9.25}$$

where L is the Obukhov length. For statically unstable conditions, surface-layer similarity theory yields

$$\Phi_M = 1 - 15\left(\frac{z}{L}\right)^{-1/4} \tag{9.26}$$

Exercise 9.4 Integrate Eq. (9.25) to derive an expression for wind speed as a function of height under statically stable conditions, assuming that $V = 0$ at $z = z_0$ and u_* and L are constant.

Solution: Separate variables:

$$dV = \frac{u_*}{k}\left[\frac{dz}{z} + \frac{8.1}{L}dz\right]$$

Then integrate to obtain

$$V - 0 = \frac{u_*}{k}\left[\ln z - \ln z_0 + \frac{8.1}{L}(z - z_0)\right]$$

Upon rearranging, this can be written as a dimensionless wind speed versus a dimensionless height

$$\frac{V}{u_*} = \frac{1}{k}\left[\ln\frac{z}{z_0} + 8.1\,\frac{(z - z_0)}{L}\right]$$

Thus, wind varies both logarithmically and linearly with height; hence, the vertical wind profile observed under stable conditions is said to be *log-linear*. ■

Vertical profiles of wind speed for stable, neutral, and unstable profiles are plotted in Fig. 9.17 on linear and logarithmic height scales. Just above the Earth's surface wind speed increases more rapidly with height in the unstable profile than in the stable profile because the more vigorous turbulence that occurs under unstable conditions is more effective at mixing momentum downward. For statically stable surface layers, the turbulence is not strong enough to homogenize the surface layer: in effect, the winds above the surface layer are decoupled from the drag at the ground.

Turbulence communicates drag from the ground throughout the middle part of the mixed layer during daytime, resulting in homogenized, uniform wind speed with height that is slower than geostrophic (i.e., *subgeostrophic*) and which crosses the isobars at a small angle toward lower pressure. Above the capping inversion or entrainment zone, winds quickly recover to their full *geostrophic* values because there is no turbulence there to communicate surface drag information. Thus, wind shear tends to be concentrated in both the surface layer (SL) and the entrainment zone (EZ), as sketched in Fig. (9.16).

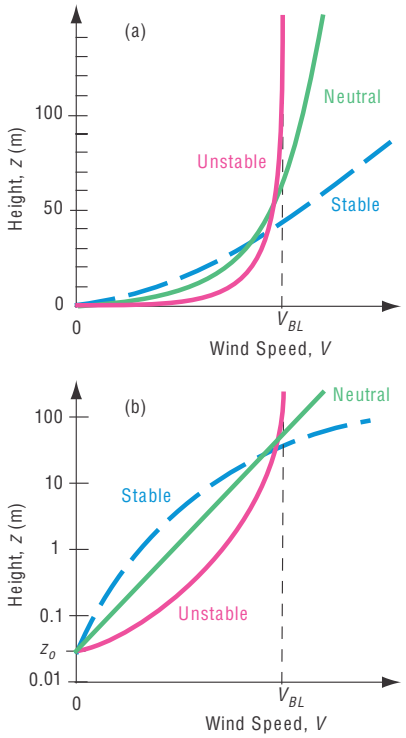

Fig. 9.17 Typical variation of wind speeds with height in the surface layer for different static stabilities, plotted on (a) linear and (b) semi-log graphs. From *Meteorology for Scientists and Engineers*, A Technical Companion Book to C. Donald Ahrens' Meteorology Today, 2nd Ed., by Stull, p. 77. Copyright 2000. Reprinted with permission of Brooks/Cole, a division of Thomson Learning: www.thomsonrights.com. Fax 800-730-2215; and from R. B. Stull, An Introduction to Boundary Layer Meteorology, Kluwer Academic Publishers, Dordrecht, The Netherlands, 1988, Fig. 9.5, p. 377, Copyright 1988 Kluwer Academic Publishers, with kind permission of Springer Science and Bussiness Media.]

At night, the suppression of turbulence by the stable boundary layer causes the air in the residual layer to suddenly be frictionless. This residual-layer air accelerates toward geostrophic, but due to the *Coriolis force* undergoes an *inertial oscillation* in which the wind vector oscillates around the geostrophic wind speed. The winds become faster than geostrophic (*supergeostrophic*) during a portion of the inertial oscillation, causing a low-altitude wind-speed maximum, called the *nocturnal jet*, which is a type of *low-level jet*. Meanwhile, closer to the

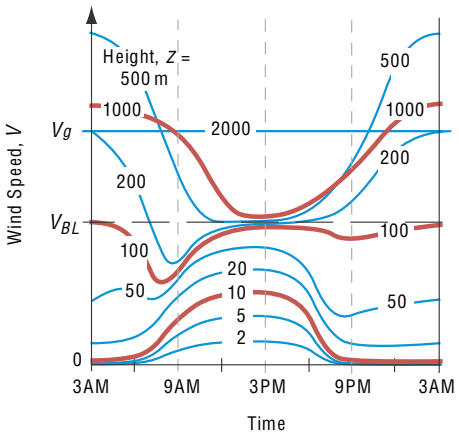

Fig. 9.18 Sketch of variation of wind speed (V) with local time on a sunny day over land, as might be measured at different heights (2 m, 5 m, 10 m . . . . 2000 m) in the boundary layer. V_g is the geostrophic wind. V_{BL} is the mixed layer wind speed, as also sketched in Fig. 9.16. [Adapted from *Meteorology for Scientists and Engineers*, A Technical Companion Book to C. Donald Ahrens' Meteorology Today, 2nd Ed., by Stull, p. 77. Copyright 2000. Reprinted with permision of Brooks/Cole, a division of Thomson Learning: www.thomsonrights.com. Fax 800-730-2215.

ground, the winds become nearly calm because the air is affected by drag at the ground, but is no longer subject to turbulent mixing of stronger winds from aloft because turbulence has diminished. Figure 9.18 shows the diurnal variation of wind speed at various heights within an idealized boundary layer.

9.3.4 Day-to-Day and Regional Variations in Boundary-Layer Structure

We have seen that over land the structure of the boundary layer exhibits a pronounced diurnal cycle in response to the alternating heating and cooling of the underlying surface. Superimposed upon these diurnal variations are day-to-day and longer timescale variations associated with changing weather patterns. Examples include: the flow of cold air over a warmer land surface following the passage of a cold front renders the bottom of the boundary layer more unstable; cloud cover suppresses the diurnal temperature range; and the passage of an anticyclone favors strong nighttime inversions. Day-to-day variations in boundary-layer structure are most pronounced during winter, when the daytime insolation is relatively weak, and during periods of unsettled weather.

Over the oceans, where the diurnal temperature variations are much weaker than over land, the air temperature is closer to being in equilibrium with the underlying surface. With a few notable exceptions,[8] air-sea temperature differences are limited to 1–2 °C. The distribution of the fluxes of latent and sensible heat at the air-sea interface is determined not by the radiation budget, but by the orientation of the low-level wind field relative to the isotherms of sea surface temperature. Over most of the area of the oceans, the flow is across the isotherms from colder toward warmer water so that the air is colder than the underlying surface and boundary layer tends to be weakly unstable, giving rise to a well-defined mixed layer similar to the one in the daytime profiles in Fig. 9.16.

Large expanses of cold advection are evident in the January climatological-mean chart shown in Fig. 9.19. The most prominent of these are off the coasts of Japan and the eastern United States, where

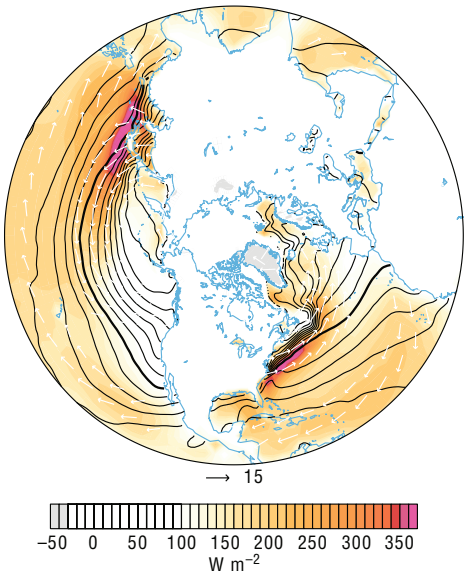

Fig. 9.19 Climatological-mean January latent plus sensible heat fluxes leaving the surface. [Based on data from data by the European Center for Medium Range Weather Forecasting 40-Year Reanalysis. Courtesy of Todd P. Mitchell.]

[8] During wintertime cold air outbreaks, cold continental air flows over the warm waters of the Gulf Stream and Kuroshio currents, giving rise to locally strong fluxes of latent and sensible heat, as discussed in connection with Fig. 9.14.

cold continental air flows over the warm western boundary-currents (i.e., the Kurishio current and the Gulf Stream, respectively). The combined sensible and latent heat fluxes in these zones (indicated by the colored shading in Fig. 9.19) are ~300 W m^{-2} in the climatological mean and they are even larger and during cold air outbreaks. The trade wind belts, where cool air is flowing equator-ward and westward over progressively warmer water, also exhibit a weakly unstable boundary-layer stratification and enhanced sensible and latent heat fluxes.

Stably stratified marine boundary layers, with vertical temperature moisture and wind profiles analogous to the nighttime land profiles in Fig. 9.16, are observed in regions of warm advection, where warm air is flowing over colder water. For example, as air that has resided over the Gulf Stream flows northward over the cold Labrador Current to the southeast of Nova Scotia (see Fig. 2.5) it becomes stably stratified. Under these conditions, the air just above the surface is often chilled to its dew point, resulting in widespread fog. *Advection fog* is also common when air approaching the coast of California passes over the narrow zone of coastal upwelling just offshore, and when warm, humid air masses off the Gulf of Mexico flow northward over snow-covered ground in the midwestern United States during winter.

Over the Arctic and Antarctic, the boundary layer becomes highly stratified in response to the uninterrupted radiative cooling of the surface during the extended polar night. Under conditions of light winds, boundary-layer turbulence virtually disappears and the capping inversion settles to the ground. Under these conditions the surface air temperature may be more than 20 °C lower than the air temperature at the top of the inversion just tens or hundreds of meters above the ground. The surface air temperature may rise sharply whenever the wind speed picks up, mixing warmer air downward from above the inversion or when a cloud layer moves overhead, increasing the downward flux of longwave radiation incident on the Earth's surface.

During cold, calm intervals, Arctic cities and towns such as Fairbanks, Alaska, experience episodes of ice fog when water vapor emitted by automobiles and wood stoves is trapped below the inversion. The frost point of the air is so low that even the emissions from a small urban complex are sufficient to supersaturate the air, resulting in the formation of tiny, sparsely distributed ice crystals referred to by local residents as "diamond dust" because of the way they sparkle in the sunlight.

9.3.5 Nonlocal Influence of Stratification on Turbulence and Stability

Based on the environmental sounding it is possible to make inferences about the vertical distribution of turbulence. In the analysis in Section 3.6, layers were examined individually and judged to be convective or nonconvective depending on the local stratification of temperature and moisture. This approach yields useful information in some cases, but it can sometimes yield misleading results because it fails to take account of the nonlocal character of turbulence.

For example, the local method would incorrectly identify the middle of the mixed layer as statically neutral (implying only moderate, isotropic turbulence and coning of smoke plumes), as opposed to statically unstable (strong turbulence, highly anisotropic, with looping smoke plumes), as demonstrated in Fig. 9.20.

The analysis of soundings can be extended to include non-local influences of stratification in the following manner.

1. First, locate any statically *unstable* regions. This is done by first plotting the θ profile. Then, from every relative maximum in θ, a

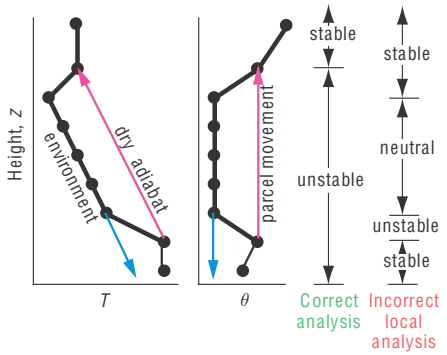

Fig. 9.20 Demonstration of how to properly determine static stability by considering nonlocal air-parcel movement from the relative maxima and minima in the potential temperature θ sounding. T is air temperature. [Adapted from *Meteorology for Scientists and Engineers*, A Technical Companion Book to C. Donald Ahrens' Meteorology Today, 2nd Ed., by Stull, p. 131. Copyright 2000. Reprinted with permission of Brooks/Cole, a division of Thomson Learning: www.thomsonrights.com. Fax 800-730-2215.]

conceptual air parcel is lifted adiabatically until it hits the sounding again (or reaches the highest altitude plotted, whichever is lower). The altitude range from start to end of this lift is statically unstable. Similarly, every relative minimum in θ is located, and a conceptual air parcel is lowered until it hits the sounding again (or hits the ground, whichever is higher). This delineates additional regions of unstable air. The total domain of unstable air is the superposition of all the unstable regions (see Fig. 9.20 for example).

2. Next, for only those subdomains outside of the unstable regions, identify as statically *stable* those regions in which $\partial\theta/\partial z > 0$.
3. Finally, designate any remaining subdomains as statically *neutral* (i.e., regions in which $\partial\theta/\partial z \simeq 0$).

In cloudy regions, the nonlocal method is applicable by changing from dry to moist adiabats when following rising air parcels above their LCL, and changing from moist to dry adiabats when following descending parcels below their LCL.

To determine regions of turbulence, regions of statically unstable air must first be estimated, using nonlocal methods as outlined earlier. Then the Richardson number criterion discussed in Section 9.1.3 is used to identify regions of dynamically unstable air. Finally, turbulence is expected in regions that are statically *or* dynamically unstable. Laminar flow is expected only where the flow is both statically *and* dynamically stable.

Exercise 9.5 A rawinsonde sounding through the lower troposphere gives the following profile information. Which layers of air are turbulent, and why?

z (km)	T (°C)	U (m s^{-1})
13	−58	30
11	−58	60
8	−30	25
5	−19	20
3	−3	18
2.5	1	9
2	2	8
1.6	0	5
0.2	13	5
0	18	0

Assume $V = 0$, $q = 0$, and $T_v = T$.

Solution: To determine the regions in which turbulence is occurring we need to examine both dynamic stability and nonlocal static stability. For dynamic stability, when the derivatives in Eq. (9.8) are approximated with finite differences, the result is called the *bulk Richardson number*

$$R_B = \frac{\dfrac{g}{\langle T_v \rangle}\Delta\theta_v \cdot \Delta z}{(\Delta U)^2 + (\Delta V)^2}$$

where the angle brackets $\langle T_v \rangle$ represent the average across the whole layer. Also, use $\theta = T + \Gamma z$, where $\Gamma = 9.8\,°\text{C km}^{-1}$ is the dry adiabatic lapse rate.

The results are in the following tables:

z (km)	T (°C)	U (m s^{-1})	θ (°C)	T_{avg} (k)	Δz (m)	ΔU (m s^{-1})	$\Delta\theta$ (K)
13	−58	30	69.4				
11	−58	60	49.8	215.15	2000	−30	19.6
8	−30	25	48.8	229.15	3000	35	1.4
5	−19	20	30	248.65	3000	5	18.4
3	−3	18	26.4	262.15	2000	2	3.6
2.5	1	9	25.5	272.15	500	9	0.9
2	2	8	21.6	274.65	500	1	3.9
1.6	0	5	15.68	274.15	400	3	5.92
0.2	13	5	14.96	279.65	1400	0	0.72
0	18	0	18	288.65	200	5	−3.04

For static stability, plot the profile, and lift parcels from every relative maximum and lower from every relative minimum to identify statically unstable regions. The layer $z = 0$ to 1.8 km is statically unstable.

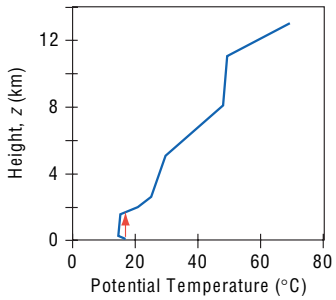

Now we consider the dynamic stability using the bulk Richardson number criterion.

Layer (km)	R_B	Dynamically	Statically	Turbulent
11 to 13	1.98	Stable	Stable	no
8 to 11	0.15	Unstable	Stable	yes
5 to 8	87.02	Stable	Stable	no
3 to 5	67.29	Stable	Stable	no
2.5 to 3	0.20	Unstable	Stable	yes
2 to 2.5	69.58	Stable	Stable	no
1.6 to 2	9.41	Stable	Unstable to 1.8 km	yes to 1.8 km
0.2 to 1.6	$+\infty$	(undefined)	Unstable	yes
0 to 0.2	-0.83	Unstable	Unstable	yes

Summary: The bottom turbulent region 0–1.8 km is the boundary layer. *Clear air turbulence* (CAT) exists near the jet stream, from 8 to 11 km. The other turbulent region is 2.5 to 3 km. ■

9.4 Evolution

This section considers the processes that control the depth of the boundary layer and cause it to evolve in response to changing environmental conditions.

9.4.1 Entrainment

The capping inversion is not a solid boundary. Hence, when rising thermals and turbulent eddies from the mixed layer reach the capping inversion, the inertia of the thermals and eddies causes them to overshoot a small distance through the capping inversion before sinking back into the mixed layer. During this overshoot, the air inside these thermals and eddies has temporarily left the mixed layer, and the pressure gradient created by the incursion of the thermal into the capping inversion drives wisps of free atmosphere air downward through the capping inversion to take the place of the missing air in the mixed layer.

But this exchange is asymmetric. The thermals overshoot into a laminar region of air in the free atmosphere, where nothing prevents these thermals (in which the air is lower in potential temperature than the air in the free atmosphere) from sinking back into the mixed layer. However, the wisps of free atmosphere air that were pushed down into the mixed layer find themselves immediately torn and mixed into the mixed layer by the strong turbulence there. These air parcels become one with the mixed layer and never return to the free atmosphere. This process is called *entrainment*, and the layer in which it takes place is called the *entrainment zone*. Entrainment occurs whenever air from a nonturbulent region is drawn into an adjacent turbulent region. It is a one-way process that adds air mass to the turbulent mixed layer. It can be thought of as a mixed layer that gradually eats its way upward into the overlying air.

Figure 9.21 shows the typical evolution of the boundary layer during fair weather over land in summer. By the end of the night, the boundary layer often consists of a stably stratified shallow boundary layer near the ground (called the *noctural boundary layer*), above which is a nearly neutral layer called the *residual layer*. Above that is the capping inversion as was shown in Figs 9.15 and 9.16.

After sunrise, the warmed ground heats the air touching the ground, creating shallow thermals that

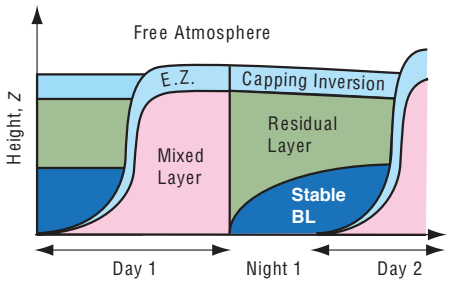

Fig. 9.21 Vertical cross section of boundary-layer structure and its typical evolution during summer over land under fair-weather, cloud-free conditions. E.Z. indicates the entrainment zone. [Adapted from *Meteorology for Scientists and Engineers*, A Technical Companion Book to C. Donald Ahrens' Meteorology Today, 2nd Ed., by Stull, p. 69. Copyright 2000. Reprinted with permission of Brooks/Cole, a division of Thomson Learning: www.thomsonrights.com. Fax 800-730-2215.]

rise and cause intense mixing (creating the *mixed layer*), and which cause entrainment at the top of the mixed layer (in the *entrainment zone*). As the mixed layer (or *convective boundary layer*) grows by entrainment, it can "burn off" the nocturnal inversion and then rapidly rise through the residual layer. Once it hits the capping inversion, the entrainment zone becomes the new capping inversion during the rest of the day.

Around sunset (Fig. 9.21), longwave radiation cools the ground to temperatures less than the overlying air temperature, and two things happen.

1. Thermals cease, allowing turbulence to decay in the former mixed layer. This former mixed layer is now called the *residual layer* because it contains the residual moisture, heat, and pollutants, as was discussed in Fig. 9.16.
2. The cold surface cools the air near the ground, transforming the bottom of the residual layer into a gradually deepening, nocturnal stable boundary layer.

Then the cycle repeats itself, day after day, as long as the weather remains fair. In winter, when the nights are longer than the days, the stable nocturnal boundary layer is much thicker, and the daytime mixed layer is so shallow that the top of the stable boundary layer persists day and night as the capping inversion.

9.4.2 Boundary-Layer Growth

The mixed layer is not a closed system with a fixed mass per unit area. It can incease in depth as air is entrained into it from above, and it can increase or decrease in depth in response to the large-scale vertical velocity; that is

$$\frac{dz_i}{dt} = w_e + w_i \tag{9.27}$$

where w_e is called the *entrainment velocity* (always nonnegative), defined as the volume of air entrained per unit horizontal area per unit time, and w_i is the vertical velocity of the large-scale motion field at the top of the boundary layer (negative for subsidence).

Exercise 9.30 shows that

$$w_i \simeq -z_i\{\nabla \cdot \mathbf{V}\} \tag{9.28}$$

where $\{\nabla \cdot \mathbf{V}\}$ is the mass-weighted divergence within the boundary layer. Over regions of fair weather, w_i is usually downward (negative) and the horizontal flow within the boundary layer is divergent. Divergence may be viewed as thinning the boundary layer over a given region by removing air laterally. Conversely, in regions of large-scale ascent, boundary layer convergence thickens the boundary layer.

A strengthening of the turbulence in the mixed layer causes greater entrainment, whereas a strengthening of the capping inversion $\Delta\theta$ reduces entrainment by reducing the inertial overshoot of the thermals and eddies. The rate of generation of *TKE* by buoyancy is proportional to the *surface sensible heat flux* F_{Hs} (in kinematic units) so the entrainment rate for a free-convective mixed layer is well approximated by

$$w_e = \frac{A\,F_{Hs}}{\Delta\theta} \tag{9.29}$$

where

$$A = -F_{Hzi}/F_{Hs} \tag{9.30}$$

The so-called *Ball parameter A* is on the order of 0.2 for free convection and increases as more mechanical turbulence adds to the entrainment.

The sensible heat flux across the capping inversion F_{Hzi} is usually negative because air with higher potential temperature from the free atmosphere is drawn downward by entrainment. An idealized sensible heat-flux profile under conditions of free convection is shown in Fig. 9.22. The average potential temperature

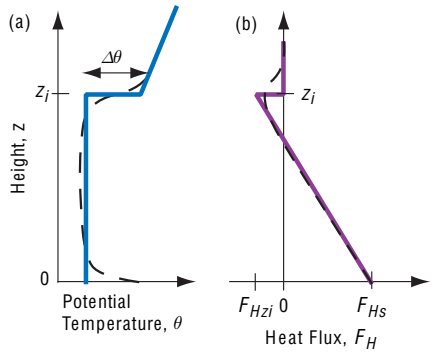

Fig. 9.22 Typical (dashed) and idealized (solid) vertical profiles of potential temperature θ and turbulent sensible heat flux F_H across the mixed layer. The idealized version is sometimes called a *slab model* (because of the uniform θ in the mixed layer) or a *jump model* (because of the discontinuity $\Delta\theta$ in the entrainment zone). [Adapted from *Meteorology for Scientists and Engineers*, A Technical Companion Book to C. Donald Ahrens' Meteorology Today, 2nd Ed., by Stull, p. 69. Copyright 2000. Reprinted with permission of Brooks/Cole, a division of Thomson Learning: www.thomsonrights.com. Fax 800-730-2215.]

in the mixed layer, $\langle\theta\rangle$, is warmed by both the upward sensible heat flux from the surface and from the downward entrainment heat flux at the top

$$\frac{d\langle\theta\rangle}{dt} = \frac{F_{Hs} - F_{Hzi}}{z_i} = \frac{(1 + A)F_{Hs}}{z_i} \tag{9.31}$$

The entrained air brings with it the heat, moisture, pollutants, and momentum from the free atmosphere. The rates at which these scalar variables are added to the boundary-layer air (per unit area) can be represented as fluxes at the top of the mixed layer. For example, for moisture

$$\overline{w'q'} = -w_e \Delta q \tag{9.32}$$

where q is specific humidity and Δq is the humidity step across the mixed-layer top ($\Delta q = q_{zi+} - q_{zi-}$). Subscripts $zi+$ and $zi-$ refer to just above and below the entrainment zone, respectively. Equations analogous to (9.32) can be written for any scalar variable, including potential temperature and pollutants, and is also used for the horizontal momentum components u and v. When existing pollutants are mixed down from elevated layers in the residual layer or free atmosphere, the process is called *fumigation*.

Under light wind conditions it is possible to predict the growth of z_i in the diurnal cycle over land based on the early morning temperature sounding and a prediction of the surface sensible kinematic heat flux. Figure 9.23a shows the idealized surface sensible heat-flux evolution, which can be predicted based on a knowledge of the day of the year (which determines sun angles) and the expected cloud coverage. Between the time shortly after sunrise when heat flux becomes positive and the time of day of interest for determining z_i, the amount of accumulated heating is the area under the curve between those two times (the hatched area in Fig. 9.23a). If advection is negligible, it can be assumed that this heat warms the boundary layer.

Assuming an adiabatic temperature profile in the mixed layer, the amount of heat needed to raise z_i from the surface to the level it reaches at $t = t_1$ is the area under the sounding (the hatched area in Fig. 9.23b). The solution is obtained by finding an average potential temperature in the mixed layer, $\langle\theta\rangle$, such that the hatched area under the sounding curve equals the hatched area under the heat-flux curve. Then, knowing $\langle\theta\rangle$, the mixed-layer depth z_i is the height at which $\langle\theta\rangle$ intersects the morning sounding. This procedure is called the *thermodynamic method* or the *encroachment method*.

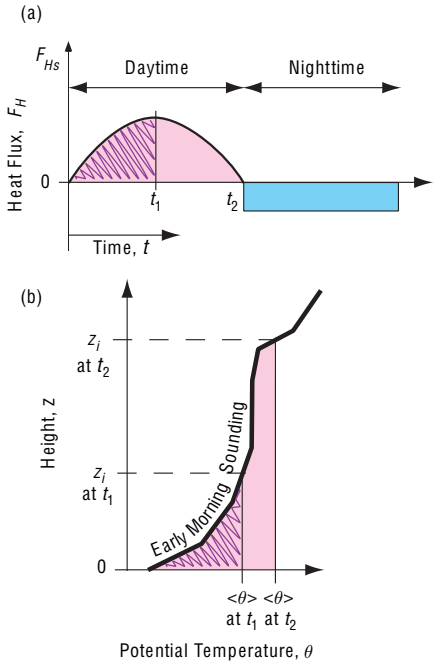

Fig. 9.23 (a) Idealized variation of surface sensible heat flux F_{Hs} (in kinematic units of K m s^{-1}) with time during fair weather over land. The area indicated by the hatched region represents the total amount of heat input into the bottom of the boundary layer from sunrise until time t_1. (b) Typical early morning sounding (heavy line) of potential temperature, θ, showing the change in the mixed-layer average potential temperature, $\langle\theta\rangle$, and depth z_i with time t. The hatched area in (a) equals the hatched area in (b). [Adapted from *Meteorology for Scientists and Engineers*, A Technical Companion Book to C. Donald Ahrens' Meteorology Today, 2nd Ed., by Stull, p. 70, 74. Copyright 2000. Reprinted with permission of Brooks/Cole, a division of Thomson Learning: www.thomsonrights.com. Fax 800-730-2215.]

Exercise 9.6 (a) If the potential temperature profile is linear in the stable boundary layer at sunrise, derive an equation for the growth rate of the mixed layer using the thermodynamic approach. For simplicity, assume the surface heat flux is constant. (b) How does the shape of this curve relate to the initial mixed-layer growth phase?

Solution: (a) If the early morning sounding is $\partial\theta/\partial z = \gamma$, and the surface kinematic heat flux is F_{Hs}, then the area under the heat-flux curve is $A = F_{Hs}\, t$,

where t is time since sunrise. The area under the sounding is a triangle, yielding $A = (\Delta\theta)^2/(2\gamma)$, where $\Delta\theta$ is the amount of warming of the mixed layer since sunrise, assuming, as initial conditions, that $z_i = 0$ at sunrise. Equating the two areas gives $\Delta\theta = (2\gamma F_{Hs} t)^{1/2}$. Because the morning profile is linear, $z_i = \Delta\theta/\gamma$. Thus, $z_i = [(2F_{Hs}/\gamma)\, t]^{1/2}$.
(b) The square root of time dependence from part (a) does not agree with the square of time dependence typically observed in the early morning, as plotted in Fig. 9.24. The difference is due to the fact that during the morning the heat flux is not constant with time, but increases sinusoidally, and also that the initial vertical profile of potential temperature is not linear, but is exponential in shape as in Fig. 9.16b. ■

9.4.3 Cloud-Topped Boundary Layer over Land

The lifting condensation level (LCL) can be below z_i on days when sufficient moisture is present in the boundary layer. In this case, the tops of the thermals that extend above the LCL are filled with cumulus clouds. During fair weather regimes over land, the cloudless boundary layer top typically rises slowly during the morning, while the noctural inversion from the previous night is being "burned off." In contrast, the LCL rises rapidly during the morning due to warming of the air near the surface, which lowers the relative humidity. Thus, the sky typically remains free of boundary-layer clouds through mid-morning because the LCL stays above the top of the rising boundary-layer.

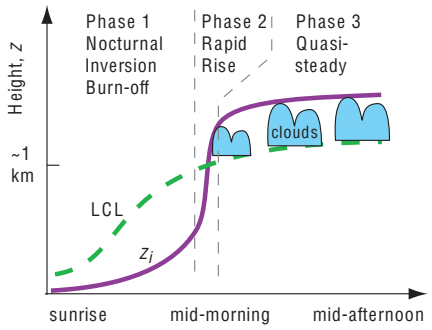

Fig. 9.24 Three-phase growth of mixed layer depth z_i during fair weather in daytime over land showing the height to which thermals can rise. Corresponding variation in the lifting condensation level (LCL) showing the heights needed by thermals to rise to produce cumulus clouds. When $z_i >$ LCL, the LCL marks the cloud base of convective clouds. [Adapted from R. B. Stull, *An Introduction to Boundary Layer Meteorology*, Kluwer Academic Publishers, Dordrecht, The Netherlands, 1988, Fig. 11.10, p. 452, and Fig. 13.12, p. 564, Copyright 1988 Kluwer Academic Publishers, with kind permission of Springer Science and Business Media.]

By late morning, the boundary layer typically experiences a rapid-rise phase after the nocturnal inversion has completely disappeared (Fig. 9.24). At around this time, z_i jumps to the height of the capping inversion from the day before (often ~1 or 2 km altitude), and becomes higher than the LCL. This is the time when fair-weather cumulus clouds are most likely to form. The degree of vertical development of the clouds depends on the height difference between the LCL (which marks the cloud base) and z_i (which marks the cloud top). These fair-weather cumulus clouds are distinguishable from the clouds associated with deep convection (see Section 8.2) because they do not penetrate beyond the top of the capping inversion into the free atmosphere. The level of the cloud top is the height to which thermals rise from the surface, and the height to which water vapor and pollutants from the surface are rapidly mixed.

Sometimes, if there is sufficient vertical wind shear $\partial V/\partial z$ in the mostly convective boundary layer, weak parallel counterrotating pairs of circulations form, which are called *horizontal roll vortices* (or "*rolls*" for short). The axes of rotation of the rolls are oriented roughly parallel with the mean wind direction, and the diameter of each roll is of the same order as the boundary-layer depth (Fig. 9.25a). These overturning circulations are almost too weak to measure, but they organize the stronger thermals into parallel lines with a spacing equal to roughly twice the boundary-layer depth. When sufficient moisture is present to support the formation of cumulus clouds, the rolls are visible as parallel rows of cumulus clouds called *cloud streets*, which are apparent in satellite images (Fig. 9.25b) and sometimes from the ground as well.

9.4.4 The Marine Boundary Layer

The cloud-topped boundary layer over the oceans tends to be different from its land counterpart in the following respects,

- Relative humidities of the surface air tend to be higher (usually in excess of 75%).
- Because of the higher relative humidity of the air, cloud cover (much of it in the form of stratus and stratocumulus cloud decks) is much more

(a)

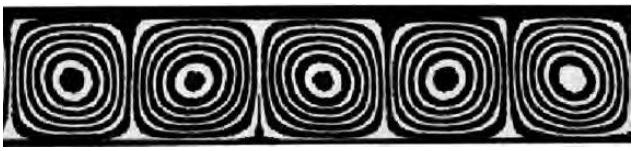

(b)

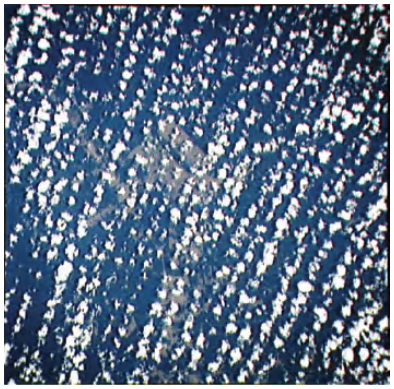

Fig. 9.25 (a) Vertical cross section through the ends of a laboratory simulation of horizontal roll vortices showing the counter-rotating circulations. [From "Influence of Initial and Boundary Conditions on Benard Convection," H.Oertel, Jr., and K. R. Kirchartz, in Recent Developments in Theoretical and Experimental Fluid Mechanics: Compressible and Incompressible Flower, U. Muller, K. G. Roesner, B. Schmidt, eds., Fig. 1, 1979, p. 356, Copyright Springer-Verlag, Berlin, 1979. With kind permission of Springer Science and Business Media.] (b) View looking down on streets of cumulus clouds aligned into rows by the horizontal roll vortices. [NASA MODIS Imagery.]

extensive. Some oceanic regions are cloud covered most of the time.

- With the widespread presence of clouds, radiative transfer plays a more important and more complex role in the boundary-layer heat balance.
- In some regions, drizzle plays a significant role in the boundary-layer heat and water balance.
- The diurnal cycle is not as important and is governed by entirely different physics.

The presence of a cloud layer tends to strengthen the capping inversion through its impact on the radiation balance of the underlying layers (i.e., the ocean plus the atmospheric boundary layer).[9] The strengthening of the capping layer, in turn, reduces the entrainment of dry air into the cloud layer, thereby contributing to the maintenance of the cloud deck. Once formed, marine cloud decks tend to persist because of this positive feedback.

In the cloud-topped boundary layer, convection may be driven by heating from below or by cooling from above. The *heating from below* is determined by the surface buoyancy flux (i.e., the sensible heat flux and the moisture flux to the extent that it affects the virtual temperature) as in the diurnal cycle over land. The *cooling from above* is determined by the flux of longwave radiation at the top of the cloud layer (see Fig. 4.30). Heating from below drives *open cell convection* (Figs. 1.21 and 9.26), with strong, concentrated, buoyant, cloudy plumes interspersed with more expansive regions of weak subsidence that are cloud-free. In contrast, cooling from above drives *closed cell convection* (Figs. 1.7 and 9.26) with strong, negatively buoyant, cloud-free downdrafts, interspersed with more expansive regions of slow ascent

[9] Where the boundary layer is shallow ($z_i \lesssim 1$ km), the reduction in insolation due to the presence of the cloud deck far outweighs the reduction in outgoing longwave radiation from the underlying water because the cloud top is not much cooler than the underlying sea surface. The net effect is radiative cooling of the mixed layer, which helps maintain clouds by keeping the relative humidity high. For boundary-layer depths ~2 km the two effects nearly cancel and the cooling is less efficient.

Fig. 9.26 Satellite photograph of mesoscale cellular convection. Open cells are in the upper-left and lower-right quadrants, and closed cells are elsewhere. [Courtesy of NASA MODIS imagery.]

that are cloudy. When satellite images of closed cell convection are rendered as negatives they resemble images of open cell convection, and vice versa. Under conditions of light winds, closed cell convection may assume the form of polygonal cells like those in a honeycomb.

In regions of strong large-scale subsidence where the boundary layer is shallow (i.e., 500 m–1 km in depth), convection-driven heating from below and cooling from above intermingle to form a unified turbulent regime that extends through the depth of the boundary layer. As the boundary layer deepens there is a tendency for the two convective regimes to become decoupled. The lower regime, driven by heating from below, is restricted to the lower part of the boundary layer. As in the daytime boundary layer over land, it may be capped by cumulus clouds.

The capping layer of the upper, radiatively driven regime coincides with the top of a more continuous stratus or stratocumulus cloud deck. The lower and upper regimes are typically separated by an intermediate quiescent layer in which the lapse rate is conditionally unstable. If the cumulus convection in the lower regime becomes sufficiently vigorous that air parcels reach their level of free convection, these buoyant thermals may rise high enough to entrain significant quantities of dry air from above the capping inversion, leading to the dissipation of the stratiform cloud deck and reunification of the turbulent layers.

We can envision the aforementioned sequence of events as occurring if we follow a hypothetical column of boundary-layer air along an equatorward trajectory along the coasts of California, Chile, or Namibia that later curves westward in the trade winds. In response to a weakening of the large-scale subsidence, the boundary layer deepens, and cumulus clouds appear below the base of the stratocumulus deck. The cumulus clouds deepen until they begin to penetrate through the overlying cloud deck. As if by magic, the dreary cloud deck thins and dissipates, leaving behind only picturesque trade wind cumulus.

Drizzle falling from the cloud deck and evaporating into the unsaturated air below it also affects the boundary-layer heat balance. The condensation of water vapor within the cloud deck releases latent heat, and the evaporation of the drizzle drops in the subcloud layer absorbs latent heat. The thermodynamic impact of the downward, gravity-driven flux of liquid water is an upward transport of sensible heat, thereby stabilizing the layer near cloud base.

Low-level cold advection contributes to the maintenance of stratiform cloud decks in two ways: it destabilizes the surface layer, thereby enhancing the flux of water vapor from the sea surface, and it cools the boundary layer relative to the overlying free atmosphere, thereby strengthening the capping inversion and reducing the entrainment of dry air. The subsidence that usually accompanies cold advection also favors a shallow boundary layer with a strong capping inversion. Hence cloud-topped boundary layers prevail in regions of climatological mean cold advection (e.g., to the east of the subtropical anticyclones) and fractional cloud coverage in these regions varies in synchrony with time variations in the strength of the cold advection.

In regions in which the marine boundary layer is topped by cloud decks, fractional cloud coverage tends to be highest around sunrise and lowest during the afternoon. The thinning (and in some cases the breakup) of the overcast during the daytime is due to the absorption of solar radiation just below the cloud tops (see Fig. 4.30). The heating at the top of the cloud deck results in a weakening of the convection within the upper part of the boundary layer, reducing the rate at which moisture is supplied from below. The moisture supply becomes insufficient to replenish the drizzle drops that rain out, and the cloud thins. The warming of the air at the cloud-top level also increases its saturation mixing ratio, thereby allowing some of the liquid water in the cloud droplets to evaporate. After the sun goes down, the air at cloud-top level cools in response to the continuing emission of longwave radiation. In response to the cooling, the convection resumes, renewing the

supply of moisture and reestablishing the population of cloud droplets.

A distinctively different kind of marine, cloud-topped boundary layer is sometimes observed during wintertime, when cold, dry continental air crosses the coastline and flows over much warmer water. Under these conditions, sea-air temperature differences may be much larger than those discussed earlier, and the boundary layer may be highly unstable. The strong sensible and latent heat fluxes at the air-sea interface drive intense convection, resulting in a pronounced warming, moistening, and thickening of the boundary layer in a matter of hours or even less over distances of tens of kilometers. This rapid transformation of the boundary layer is a dramatic example of what synoptic meteorologists refer to as *air-mass modification*.

Figure 9.27 shows cold Canadian air streaming southeastward over the Great Lakes, the eastern United States, and the warm Gulf Stream waters of the western Atlantic. As the cold air first moves over unfrozen Lake Ontario, observers standing on the upwind shore of Ontario, Canada, can observe mostly clear skies, but with *steam fog* forming a short distance over the water due to the intense heat and moisture fluxes from the lake surface into the air. As the air crosses the lake, the convective mixed layer deepens and cloud streets develop, aligned with the mean wind direction. The cloud streets widen, deepen, and change into open-cell mesoscale convection as they move downstream. A similar evolution is observed over the Gulf Stream.

Under certain conditions the moisture picked up by the air crossing a large lake can be concentrated within one or more bands of low-level convergence, aligned with the flow, that are capable of producing moderate to heavy snow where they come ashore on the lee side of the lake. Some of the more notable of these *lake-effect snow squall (LES)* events have yielded snowfall amounts in excess of 1 m, which is all the more remarkable considering that the clouds in these systems are typically only 2–3 km deep.

9.4.5 Stormy Weather

In regions of large-scale ascent (e.g., near centers of cyclones and fronts) and in deep convective clouds the mixed-layer top rises to the point where the tropopause, in effect, becomes the capping inversion (Fig. 9.28). It is in these regions that boundary-layer air, with its moisture and pollutants, is most free to mix with the air in the free atmosphere. The character of this mixing is illustrated schematically in Fig. 9.29, in which fronts are depicted as peeling the boundary layer upward along sloping surfaces, and thunderstorms act like vents or chimneys that pump boundary-layer air upward.

After a storm or frontal passage over land, such as the cold front illustrated in Fig. 9.30, the *frontal inversion* (between the top of the cold air mass and the overlying warmer air) is initially the new boundary-layer top. However, after a day or two, when the clouds have cleared and a diurnal cycle of radiative heating and cooling is once again felt by the ground, a new boundary layer forms with depth z_i below the overlying frontal inversion. Such multiple inversion layers (both mixed-layer top and frontal inversion aloft) can often be seen in upper-air soundings.

9.5 Special Effects

In the previous sections the surface underlying the boundary layer was assumed to be flat and either horizontally uniform or (when the effects of horizontal temperature advection were taken into account) slowly varying. This section considers a number of special boundary-layer phenomena that derive from special properties of the underlying surface, in particular,

- terrain,
- discontinuities such as coastines,
- texture, as in the case of forests, and
- human impacts, as in the case of cities.

9.5.1 Terrain Effects

When mountain slopes are heated by the sun during the day in fair-weather conditions, the warm air rises along the slope as an *anabatic wind*[10] (Fig. 9.31). Along a mountain crest, where anabatic winds from the the two sides of the mountain meet, the air rises above the crest and can create *anabatic cumulus clouds* if sufficient moisture is present. Associated with these upslope winds are *return circulations* that include weak downdrafts aloft in the centers of the valley.

[10] *ana*: from the Greek for upward.

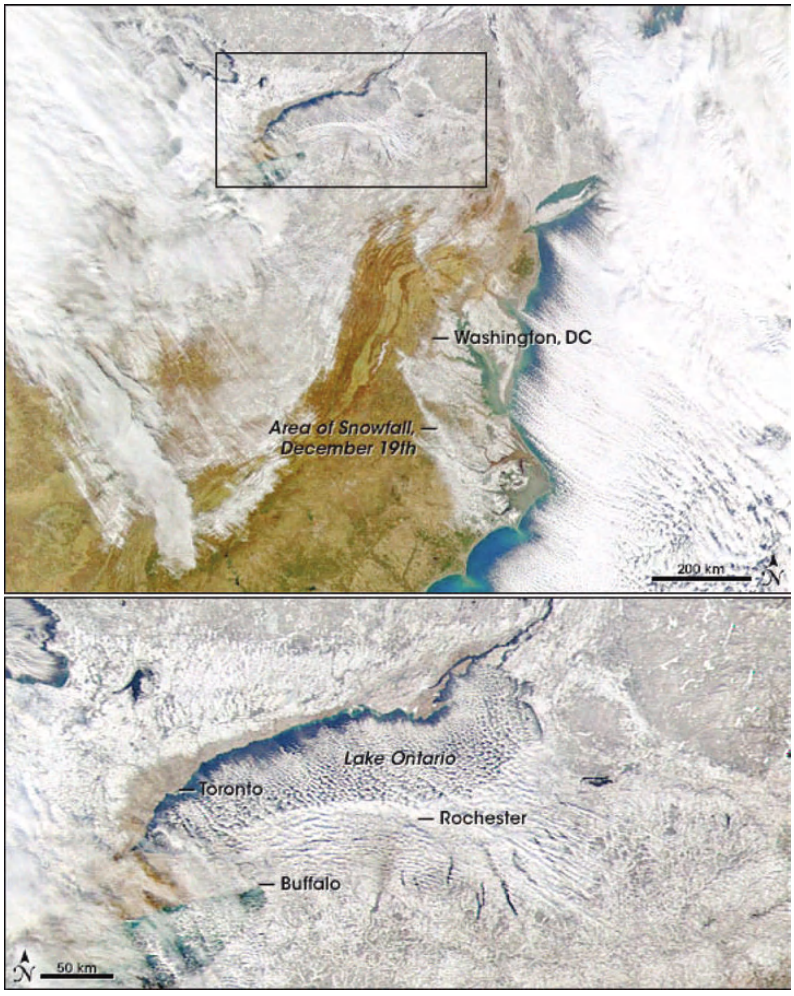

Fig. 9.27 (Top) Visible satellite image of eastern North America and the western North Atlantic showing clouds and snow-covered ground. The region near Lake Ontario outlined by the rectangle is shown in more detail in the bottom figure. Winds are from the northwest, causing cloud streets over the Great Lakes and over the Atlantic Ocean. Water vapor picked up by the air as it crossed Lake Ontario triggered a *lake effect snowstorm* downsteam over upper New York State. [NASA MODIS imagery.]

At night when the mountain slopes are cooled by longwave radiation, the chilled air sinks downslope as a cold *katabatic wind*[11] due to its negative buoyancy. This flow is compensated by a return circulation having weak rising air aloft over the valley center. The chilled air that collects as a *cold pool* in the valley floor is conducive to *fog* formation. Layers of less cooled air do not descend all the way to the valley floor, but spread horizontally at their level of neutral buoyancy, as indicated by the pink arrows in Fig. 9.31. Both the anabatic and katabatic winds are called *cross-valley circulations*.

[11] *kata:* from the Greek for downward.

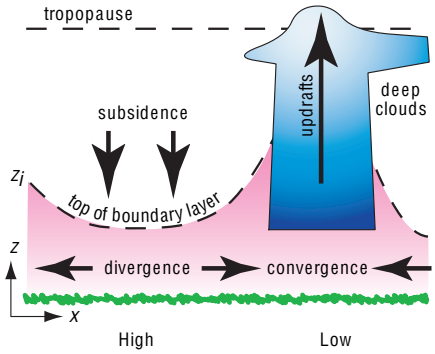

Fig. 9.28 Vertical slice through an idealized atmosphere showing variations in the boundary layer depth z_i in cyclonic (low pressure) and anticyclonic (high pressure) weather conditions. [Adapted from *Meteorology for Scientists and Engineers*, A Technical Companion Book to C. Donald Ahrens' Meteorology Today, 2nd Ed., by Stull, p. 69. Copyright 2000. Reprinted with permission of Brooks/Cole, a division of Thomon Learning: www.thomsonrights.com. Fax 800-730-2215.]

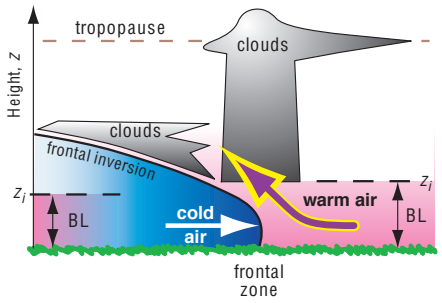

Fig. 9.30 Vertical cross section illustrating the destruction of the capping inversion z_i and venting of boundary layer (BL) air near frontal zones, and subsequent reestablishment of the capping inversion under the frontal inversion after cold frontal passage. [Adapted from *Meteorology for Scientists and Engineers*, A Technical Companion Book to C. Donald Ahrens' Meteorology Today, 2nd Ed., by Stull, p. 69. Copyright 2000. Reprinted with permission of Brooks/Cole, a division of Thomon Learning: www.thomsonrights.com. Fax 800-730-2215.]

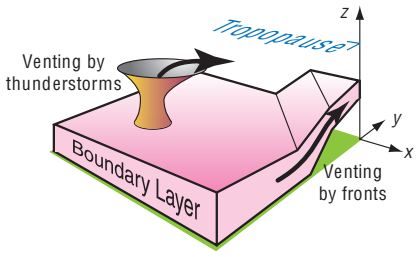

Fig. 9.29 The two dominant mechanisms for boundary-layer air to pass the capping inversion and enter the free atmosphere. [Courtesy of Roland B. Stull.]

Anabatic and katabatic flows are examples of a broader class of diurnally varying thermally driven circulations, which also include land and sea breezes described in the next subsection. Horizontal temperature gradients caused by differential solar heating or longwave cooling cause horizontal pressure gradients, as described by the hypsometric equation and the thermal wind effect. For example, over sloping terrain during the afternoon, a pressure gradient forms normal to the slope, as illustrated in Fig. 9.32. This pressure-gradient force induces an upslope (anabatic) flow during daytime, while the increased density of the air just above the surface at night induces a downslope (katabatic) flow.

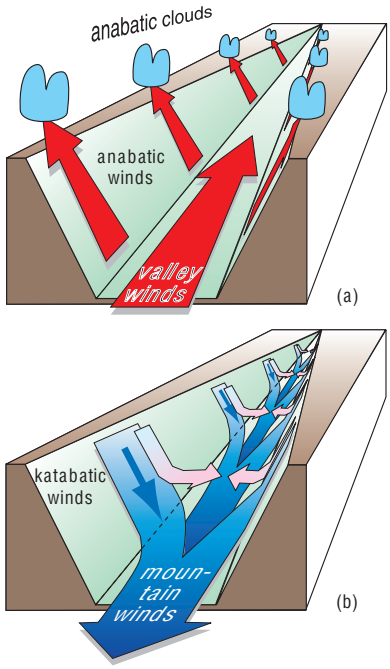

Fig. 9.31 (a) Daytime conditions of anabatic (warm upslope) winds along the valley walls, and associated valley winds along the valley floor. (b) Nighttime conditions of katabatic (cold downslope) winds along the valley walls, and associated mountain winds draining down the valley floor streambed. [Adapted from R. B. Stull, *An Introduction to Boundary Layer Meteorology*, Kluwer, Academic Publishers, Dordrecht, The Netherlands, 1988, Fig. 14.5, p. 592, Copyright 1988 Kluwer Academic Publishers, with kind permission of Springer Science and Business Media.]

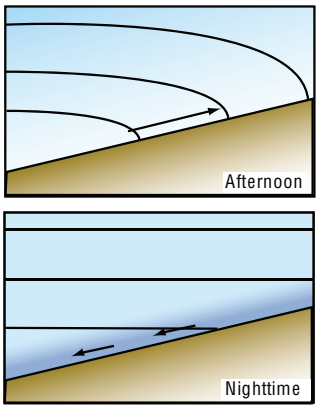

Fig. 9.32 Schematic showing how circulations develop in response to land-sea heating contrasts and heating along sloping terrain. Faded (darkened) blue shading indicates planetary boundary temperatures higher (lower) than free air temperatures at the same level. The contours show how pressure surfaces are distorted by the diurnally varying boundary layer temperatures, and arrows indicate the upslope/downslope accelerations induced by the horizontal temperature gradients.

Along-valley winds also form due to these buoyant forcings (Fig. 9.31). At night, the cold air that pools in a valley follows the streambed downslope, causing cold *mountain winds* to drain out of the mountain valleys onto broader plains. During daytime, there is an up-valley flow called the *valley wind* along the streambed.

There are times when the relatively weak, diurnally dependent, thermally driven circulations discussed in this subsection are over-shadowed by stronger winds that evolve in accordance with the synoptic-scale forcing. Strong synopic-scale pressure gradients in mountainous regions are often attended by a number of distinctive phenomena on smaller scales, including *gap winds* (Section 8.2.4), *mountain waves* and *lenticular clouds*, local accelerations of the wind over mountain crests, *blocking* of low-altitude winds, lee-side "*cavity*" circulations, *rotor clouds, banner clouds, wake turbulence, Karman vortex streets*, downslope wind storms, and *hydraulic jumps* (Fig. 9.33). Even low hills can exert a surprisingly strong influence on cloud patterns (Fig. 9.34) and precipitation amounts.

A nondimensional parameter that is widely used to characterize the flow over mountains and to predict

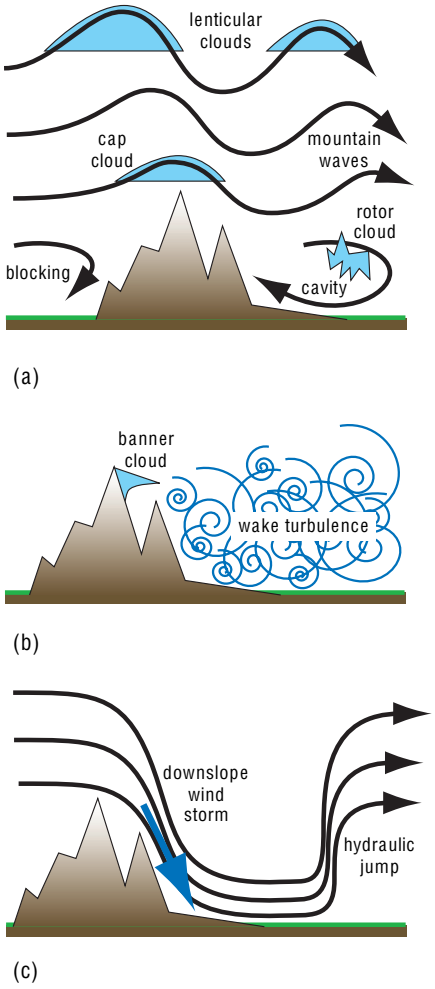

Fig. 9.33 Vertical cross-section sketches of some of the phenomena observed in mountains during windy conditions. [Adapted from R. B. Stull, *An Introduction to Boundary Layer Meteorology*, Kluwer, Academic Publishers, Dordrecht, The Netherlands, 1988, Fig. 14.4, p. 602, and Fig. 14.9, p. 608, Copyright 1988 Kluwer Academic Publishers, with kind permission of Springer Science and Business Media.]

the kinds of flow configurations that might occur is the *Froude*[12] *number*

$$Fr = \frac{V}{NS} \tag{9.33}$$

[12] **William Froude** (1810–1879) British hydrodynamicist, engineer, and naval architect who studied water resistance of scale-model ships in towing tanks under contract to the British Navy. Developed an understanding of skin roughness drag versus wave drag and studied ship stability to improve safety and efficiency. Developed the Froude number ratio of inertial to buoyancy forces as a way to scale his model results to full-size ships. Invented a hydraulic dynameter to measure the output of high-powered ship engines.

Fig. 9.34 Cloud streets organized by flow over a nearby ~130-m-high hill. Each photograph was taken on a different day, but the winds on all 3 days were blowing from nearly the same direction. [Photographs courtesy of Art Rangno.]

where V is the wind speed component normal to the mountain, N the Brunt-Väisälä frequency, and S, the vertical (or, for some applications, horizontal) scale of the mountain. The Froude number can be interpreted as the natural wavelength of the buoyancy oscillations, discussed in Exercise 3.13, divided by the wavelength of the mountain. The square of Fr is like a kinetic energy of the incident flow divided by the potential energy needed to lift air over the mountain.

For small values of Fr, the low-level airflow is forced to go around the mountain and/or through gaps. Larger values of Fr are associated with more flow over the top of the mountain. From the results of Exercise 3.13 it is clear that if S is defined as the horizontal wavelength of a sinusoidal mountain range with ridges perpendicular to the flow, the wavelength of the waves induced by flow over the mountain range is proportional to Fr. In the real world, V and N vary with height and the topography of mountain ranges is a two-dimensional function that is often too complex to characterize by a single height or width scale. Hence, to perform realistic simulations of terrain effects requires the use of numerical or laboratory models.

9.5.2 Sea Breezes

Diurnal temperature ranges at the Earth's surface in excess of 15 °C are commonly observed over land in the tropics and in middle latitudes of the summer hemisphere, where daytime insolation is strong. Over land, the low thermal conductivity of the soil tends to concentrate the response within a thin layer just below the surface, as was illustrated in Fig. 9.12. Hence, land surfaces react much more quickly to changes of insolation than the ocean surface. It follows that the continents tend to be warmer than the oceans during the afternoons and they cool off more at night due to the emission of infrared radiation. The resulting land-sea temperature contrasts cause horizontal pressure gradients that drive shallow, diurnally varying, circulations: daytime sea breezes and nighttime land breezes.

A *sea breeze* is a cool shallow wind that blows onshore (from sea to land) during daytime. It occurs during weak background synoptic forcings (i.e., weak or calm geostrophic wind) under generally clear skies and is caused by a 5 °C or greater temperature contrast between the sun-heated warm land and the cooler water. Analogous flows called *lake breezes* form along lake shorelines, while *inland sea breezes* form along boundaries between adjacent land regions with different surface characteristics (e.g., deserts versus vegetated terrain). The sea breeze is a surface manifestation of a thermally driven mesoscale circulation called the *sea-breeze circulation*, which often includes a weak return (land to sea) flow aloft (Fig. 9.35).

A *sea-breeze front* marks the leading edge of the advancing cool marine air and behaves similarly to a weak advancing cold front or a thunderstorm gust front. If sufficient moisture is present in the updraft ahead of the front, a line of cumulus clouds can form along the front, and a line of thunderstorms can be triggered if the atmosphere is convectively unstable. The raised portion of cool air immediately behind the front, called the *sea-breeze head*, is analogous to the head at the leading edge of a gust front (Section 8.3.3c). The sea-breeze head is roughly twice as thick as the subsequent portion of the *feeder* cool onshore flow (which is ~0.5 to 1 km thick). The top of the

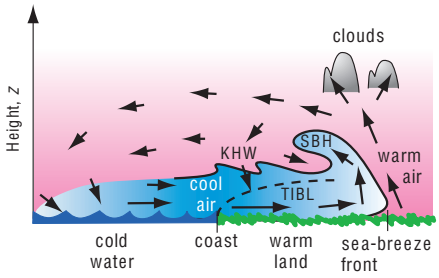

Fig. 9.35 Components of a sea-breeze circulation. SBH, sea-breeze head. KHW, Kelvin–Helmholtz waves. The top of the thermal internal boundary layer (TIBL) is shown by the dashed line. [Adapted from R. B. Stull, *An Introduction to Boundary Layer Meteorology*, Kluwer Academic Publishers, Dordrecht, The Netherlands, 1988, Fig. 14.7, p. 594, Copyright 1988 Kluwer Academic Publishers, with kind permission of Springer Science and Business Media.]

sea-breeze head often curls back over warmer air from aloft in a large horizontal roll eddy.

Vertical wind shear at the density interface between the low-level sea breeze and the return flow aloft can give rise to Kelvin-Helmholtz waves with wavelength of ~0.5 to 1 km along the density interface at the top of the feeder flow behind the head. These waves increase the frictional drag on the sea breeze by entraining low-momentum air from above the interface. A slowly subsiding return flow occurs over water and completes the circulation as the air is again cooled as it blows landward over the cold water. As the cool air flows over the land, a *thermal internal boundary layer* (TIBL) forms just above the ground and grows in depth with the square root of distance from the shore as the marine air is modified by the heat flux from the underlying warm ground.

The initial sea-breeze circulation is not very wide, but spreads out over land and even farther over water as the day progresses. Advancing cold air behind the sea-breeze front behaves somewhat like a *density current* or *gravity current* in which a dense fluid spreads out horizontally beneath a less dense fluid, as has been simulated in water tanks. The sea-breeze front can advance 10 to 200 km inland by the end of the day, although typical advances are ~20 to 60 km unless inhibited by mountains or by opposing synoptic-scale winds. As the front advances, prefrontal waves may cause wind shifts ahead of the front.

When fully developed, surface (10 m height) wind speeds in the marine, inflow portion of the sea breeze at the coast range from ~1 to 10 m s^{-1} with typical values of ~6 m s^{-1}. Wind speed increases with the square root of the land-sea temperature difference. The sea-breeze front usually advances at a speed of ~87% of the surface wind speed. At the end of the day, the sea-breeze circulation dissipates and a weaker, reverse circulation called the *land-breeze* forms in response to the nighttime cooling of the land surface relative to the sea. Sometimes, the now-disconnected sea-breeze front continues to advance farther inland during the night over the growing nocturnal stable boundary layer as a *bore* (a propagating solitary wave with characteristics similar to an hydraulic jump), a phenomenon known in Australia as the *Morning Glory*.

In the plane of a vertical cross section normal to the coastline (as in Fig. 9.35) the surface wind oscillates back and forth between onshore and offshore, reversing directions during the morning and evening hours. The Coriolis force induces an oscillating alongshore wind component that lags the onshore-offshore component by 6 h (or 1/4 cycle). Hence, the diurnal wind vector rotates throughout the course of the day: clockwise in the northern hemisphere and counterclockwise in the southern hemisphere. For example, along a meridional coastline with the ocean to the west in the northern hemisphere, the diurnal component of the surface wind tends to be westerly (onshore) during the afternoon, northerly (alongshore) during the evening, and so on. The diurnal wind component and the mean (24 h average) surface wind are additive. If the mean wind in the above example is blowing, say, from the north, the surface wind speed will tend to be higher around sunset when the mean wind and the diurnal component are in the same direction, than around sunrise, when they are in opposing directions.[13,14]

Many coasts have complex shaped coastlines with bays or mountains, resulting in a myriad of interactions

[13] Irrespective of the effects described here, the wind speed often drops around or just after sunset in response to the weakening of the boundary-layer turbulence, which reduces the downward mixing of momentum.

[14] The diurnal wind vector along sloping terrain rotates in a similar manner, and the daytime strengthening and nighttime weakening of the turbulence in the land boundary layer also contribute to the diurnal cycle in boundary-layer winds. The amplitude of these oscillations tends to be largest around 30° latitude where the diurnal cycle matches the period of an inertia circle.

between local flows that distort the sea breeze and create regions of enhanced convergence and divergence. The sea breeze can also interact with boundary-layer convection, horizontal roll vortices, and urban heat islands, causing complex dispersion of pollutants emitted near the shore. If the onshore synoptic-scale geostrophic wind is too strong, a TIBL develops instead of a sea-breeze circulation.

In regions such as the west coast of the Americas, where major mountain ranges lie within a few hundred kilometers of the coast, sea breezes and terrain effects appear in combination. Figure 9.36 shows an example of how low-level convergence associated with the boundary-layer wind field influences the diurnal cycle in deep convection and rainfall over Central America. Elevated land areas along the crest of the Sierras Madre mountain range experience convection during the afternoon when the sea breeze and upslope flow conspire to produce low-level convergence. In contrast, the offshore waters experience convection most frequently during the early morning hours, in response to the convergence associated with the land breeze, augmented by katabatic winds from the nearby mountains. Morning convection is particularly strong in the Gulf of Panama because of its concave coastline. The prevalence of afternoon convection, driven by the the sea breeze circulation, is also clearly evident over the southeastern United States.

9.5.3 Forest Canopy Effects

The drag associated with *forest canopies* (i.e., the leafy top part of the trees) is so strong that the flow above the canopy often becomes partially separated from the flow below, in the trunk space. In the region above the canopy in the surface layer, the flow exhibits the typical logarithmic wind profile but with the effective aerodynamic surface displaced upward to near the canopy top (Fig. 9.37a). In the trunk space the air often has a relative maximum of wind speed between the ground and the canopy, and often these subcanopy winds flow mostly downslope both day and night if the canopy is dense.

The static stability below the canopy is often opposite to that above the canopy. For example, during clear nights, strong longwave cooling of the canopy will cause a statically stable boundary layer to form above the canopy (Fig. 9.37b). However, some of the cold air from the canopy sinks as upside-down thermals, creating a convective mixed layer in the trunk space at night that gets cooler as the night progresses. During daytime, a superadiabatic surface layer with warm convective thermals forms above the canopy, while in the trunk space the air is warmed from the canopy above and becomes statically stable (Fig. 9.37c). These peculiar configurations of static stability are successfully captured with the nonlocal method of determining static stability.

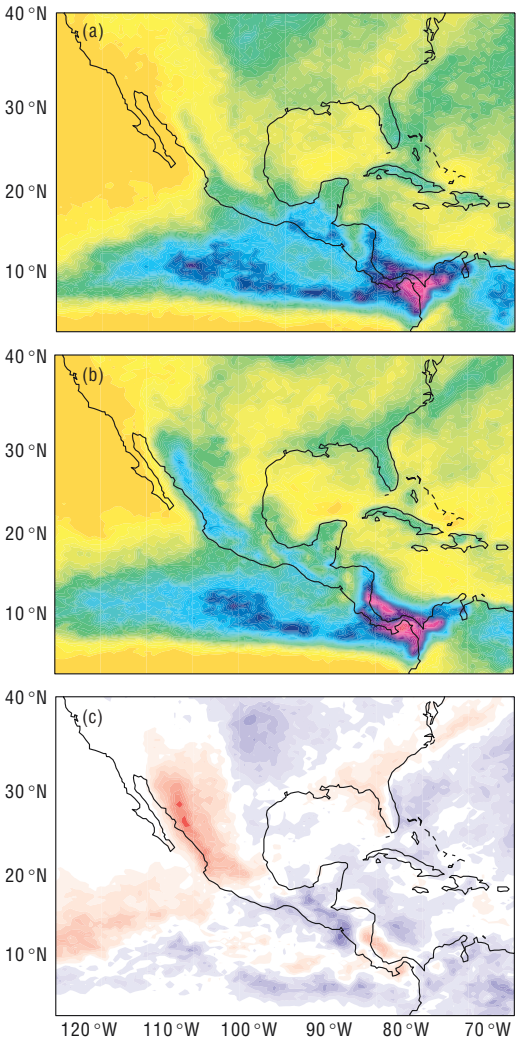

Fig. 9.36 Frequency of deep convection as indicated by clouds with tops colder than −38 °C at two different times of day during July at around (a) 5 AM local time and (b) 5 PM local time. Panel (c) shows the difference (a)–(b). Color scale for (a) and (b) analogous to that in Fig. 1.25; in (c) red shading indicates heavier precipitation at 5 PM. [Courtesy of U.S. CLIVAR Pan American Implementation Panel and Ken Howard, NOAA-NSSL.]

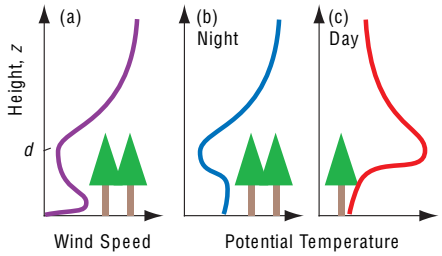

Fig. 9.37 (a) Wind speed in a forest canopy. (b) Potential temperature profile on a clear night with light winds. The level *d* represents the displacement distance of the effective surface for the logarithmic wind profile in the surface layer above the top of the canopy. (c) Same as (b), but on a sunny day. [Courtesy of Roland B. Stull.]

9.5.4 Urban Effects

Large cities differ from the surrounding rural areas by virtue of having larger buildings that exert a stronger drag on the wind; less ground moisture and vegetation, resulting in reduced evaporation; different albedo characteristics that are strongly dependent on the relationship between sun position and alignment of the *urban street canyons*; different heat capacity; and greater emissions of pollutants and anthropogenic heat production. All of these effects usually cause the city center to be warmer than the surroundings—a phenomenon called the *urban heat island* (Fig. 9.38a).

When a light synoptic-scale wind is blowing, the excess warmth and increased pollutants extend downwind as a city-scale *urban plume* (Fig. 9.38b). In some of these urban plumes the length of the growing season (days between last frost in spring and first frost in fall) in the rural areas adjacent to the city has been observed to increase by 15 days compared to the surrounding regions.

Within individual street canyons between strong buildings, winds can be funneled and accelerated. Also, as fast winds from aloft hit tall buildings, the winds are deflected downward to increase wind speeds near the base of these skyscrapers. Behind individual buildings is often a "cavity" of circulation with surface wind direction opposite to the stronger winds aloft, which can cause unanticipated transport of pollutants from the street level up to open windows. In lighter wind conditions, the increased roughness length associated with tall buildings can reduce the wind speed on average over the whole city, allowing pollutant concentrations to build to high levels.

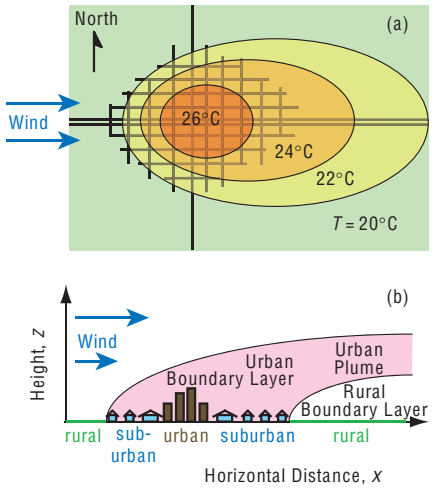

Fig. 9.38 (a) Urban heat island effect, with warmer air temperatures over and downwind of a city. Air temperature excess in the city core can be 2 to 12 °C warmer than the air upstream over rural areas. The grid of lines represents roads. (b) Vertical cross section through a city. The urban plume includes excess heat as well as increased pollution. [Adapted from T. R. Oke, *Boundary Layer Climates*, 2nd Ed., Routledge, New York (1987).]

The largest cities generate and store so much heat that they can create convective mixed layers over them both day and night during fair-weather conditions. This urban heat source is often associated with enhanced thermals and updrafts over the city, with weak return-circulation downdrafts over the adjacent countryside. One detrimental effect is that pollutants are continually recirculated into the city. Also, the enhanced convection over a city can cause measurable increases in convective clouds and thunderstorm rain.

9.6 The Boundary Layer in Context

Boundary-layer meteorology is still a relatively young field of study with many unsolved problems. The basic equations of thermodynamics and dynamics have resisted analytical solution for centuries. The Reynolds-averaging approach resorts to statistical averages of the effects of turbulence in an attempt to circumvent the intrinsic lack of predictability in the deterministic solutions of the eddies themselves. The turbulence closure problem has not been solved, and the chaotic nature of turbulence poses major challenges. Many of the useful empirical relationships,

such as the logarithmic wind profile, are founded on similarity theory, which basically ignores physics and dynamics and focuses on the dimensions of the key variables. The nature of turbulence and entrainment of ambient air into clouds is also incompletely understood, as well as the feedbacks between clouds and the fluid motions in the boundary layer.

Despite these formidable obstacles, significant advances are being made in many areas. Boundary-layer models are being coupled with larger-scale models to capture the important effects of multiscale advection. Remote sensing is used to observe the eddies and thermals that cause the turbulence, and very fine resolution computing is being used to simulate boundary-layer turbulence, as explained later.

Horizontal advection of heat, moisture, and momentum by larger-scale mean wind nearly always dominates over turbulent effects in the boundary layer, even during periods of fair weather and light winds. Also, vertical advection by the large-scale motion field is usually the same order of magnitude or larger than the turbulent entrainment at the mixed-layer top. To properly include these larger-scale advective effects, boundary-layer models are often embedded in mesoscale models, which, in turn, are nested in large-scale numerical weather prediction models.

Remote sensing has been used increasingly by researchers since the 1970s to observe the boundary layer. Clear-air radar emits microwaves to observe boundary-layer eddies, as made visible by humidity-related microwave refractivity fluctuations. *Lidar* (light detection and ranging) transmits a beam of radiation at visible or near-visible wavelengths to illuminate aerosols carried aloft by thermals (Fig. 9.39) and uses large telescopes to capture the photons scattered back to the lidar. Sodar (sound detection and ranging) emits loud pulses of sound and uses sensitive microphones to detect faint echoes scattered from regions of strong temperature gradients in and around surface-layer eddies and plumes. *Profilers* monitor the Doppler shift of pulses of off-vertically propagating radio waves, from which the wind profile can be inferred, while *RASS (radio acoustic sounding systems)* use radio waves to measure the speed of sound waves, from which the temperature profile can be inferred.

Realistic numerical simulation of boundary-layer phenomena is inherently more computationally intensive than numerical weather prediction. The range of horizontal scales is larger (in a logarithmic sense), so more grid points are needed. In addition, motions in the boundary layer tend to be fully three dimensional

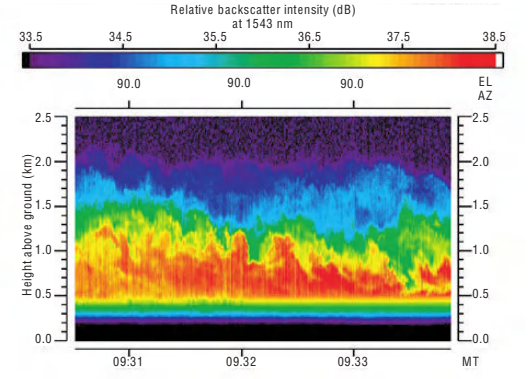

Fig. 9.39 Time-height cross section showing boundary-layer thermals (red and yellow colors) as they drift over a vertically pointing lidar. Pollution particles in the rising thermals, which backscatter light back to the lidar telescope, are rendered in red and yellow colors. Black, purple, and blue indicate air that is relatively clean in the free atmosphere. [Courtesy of Shane Mayor, National Center for Atmospheric Research.]

and nonhydrostatic so additional layers are required in the vertical as well. The timescales of microscale turbulence are orders of magnitude shorter than the timescale for phenomena such as baroclinic waves so much shorter time steps are required.

Despite these formidable computational requirements, some notable advances have been made in recent years. A particularly productive approach has been *large eddy simulation (LES)*, in which numerical weather prediction models are run on high-performance computers with ~10-m grid spacing, which is sufficient to resolve the larger, more energetic eddies. Finer resolution *direct numerical simulation (DNS)* computer models have been run over very small domains with grid spacings as fine as millimeters, which is sufficient to resolve all eddy sizes down to scales on which molecular conduction and diffusion dominate. As computer power continues to increase, DNS and LES are merging to provide direct computation of turbulent flow over arbitrarily complex terrain.

As more of these new observing and numerical-modeling capabilities come on line, it is becoming increasingly possible to transcend the limitations of statistical approaches and similarity theory by pursuing a more phenomenogically based approach to boundary-layer studies. Part of the thrill of boundary-layer research is that there are still many important phenomena and processes waiting to be discovered.

Exercises

9.7 Explain and interpret the following:

(a) Air pollution is often trapped within the boundary layer.

(b) Clear-air turbulence (CAT) experienced by airplane passengers is widespread, but usually not very strong in the boundary layer. It tends to be more sporadic and also more intense near the tropopause.

(c) Air within the free troposphere exhibits only a small diurnal temperature range.

(d) Boundary layers over deserts are often much deeper than over vegetated terrain.

(e) The warmest and highest-rising thermals often have the highest LCLs.

(f) Boundary-layer turbulence in the Earth's atmosphere decays during a solar eclipse.

(g) Birds soar during daytime over land, not usually at night.

(h) Turbulence kinetic energy is dissipated into internal energy.

(i) Convective overturning creates fat thermals with a mean diameter of order of the boundary-layer depth, as opposed to thin thermals of the width of smoke-stack plumes.

(j) The theoretical height of the LCL based on surface temperature and dew point is a very accurate predictor of the height of cloud base for convective clouds.

(k) The LCL is a poor predictor for the base height of stratus clouds.

(l) Deterministic forecasts of any scale of turbulent phenomenon are accurate out to duration roughly equal to the lifetime of individual eddies.

(m) The covariance between u and w is both the vertical flux of horizontal momentum and the horizontal flux of vertical momentum.

(n) The covariance of θ and q does not represent a flux.

(o) During day, boundary layers are often shallow near shorelines and increase with distance inland.

(p) Kelvin-Helmholtz breaking waves and turbulence occur much more often than the occurrence of billow clouds.

(q) The method of estimating turbulent transport demonstrated in Fig. 9.8 does not necessarily work for larger eddies.

(r) Zeroth-order similarity theories give useful important information, even though they contain no dynamics.

(s) Gradient-transfer theory fails in the interior of the mixed layer.

(t) What would be the opposite of the oasis effect, and could it occur in nature?

(u) Significant vertical turbulent fluxes can exist near the surface even in the limit of zero wind speed.

(v) The drag coefficient is related to the roughness length.

(w) During some nights dew will form on the ground, but on others fog forms instead.

(x) Hot-air balloonists like to take off in near-calm conditions at the surface, but can find themselves in fast-moving air a short distance above the surface.

(y) Hot-air balloonists who take off in the near-calm winds of early morning, find it much more difficult to land by mid morning because of faster winds.

(z) On a sunny day, the air in the trunk space below a forest canopy is stably stratified.

(aa) Turbulence in the residual layer decays quickly after sunset.

(bb) Greater subsidence does not inject more air into the top of the mixed layer, but has the opposite effect of making the mixed layer more shallow.

(cc) The rapid-rise phase of mixed-layer growth happens only after the nocturnal inversion has been "burned off."

(dd) The boundary layer is poorly defined near fronts.

(ee) When air flows over a change in roughness, an internal boundary layer develops. The depth of this layer grows with increasing distance from the change.

(ff) Latent and sensible heat fluxes over land surfaces tend to be larger on clear days than on cloudy days.

(gg) Daytime temperatures tend to be higher over deserts than over vegetated land surfaces.

(hh) Other conditions being the same, alpine glaciers and snow-fields lose more mass on a humid summer day than on a dry summer day.

(ii) On a clear, calm day, the surface sensible heat flux into the air does not usually become positive until 30 to 60 min after sunrise.

(jj) In fair weather, the heat and momentum fluxes at the top of the mixed layer due to entrainment are usually downward, but the moisture flux is positive.

(kk) You can estimate the static stability of the boundary layer by looking at the shape of the smoke plume from a smoke stack.

(ll) In Fig. 9.40, why do the surface wind speed and the cloudiness increase as the air flows northward across the sharp front in the sea-surface temperature field that lies along 1 °N?

9.8 Estimate the temperature variance for the velocity trace at the bottom of Fig. 9.6.

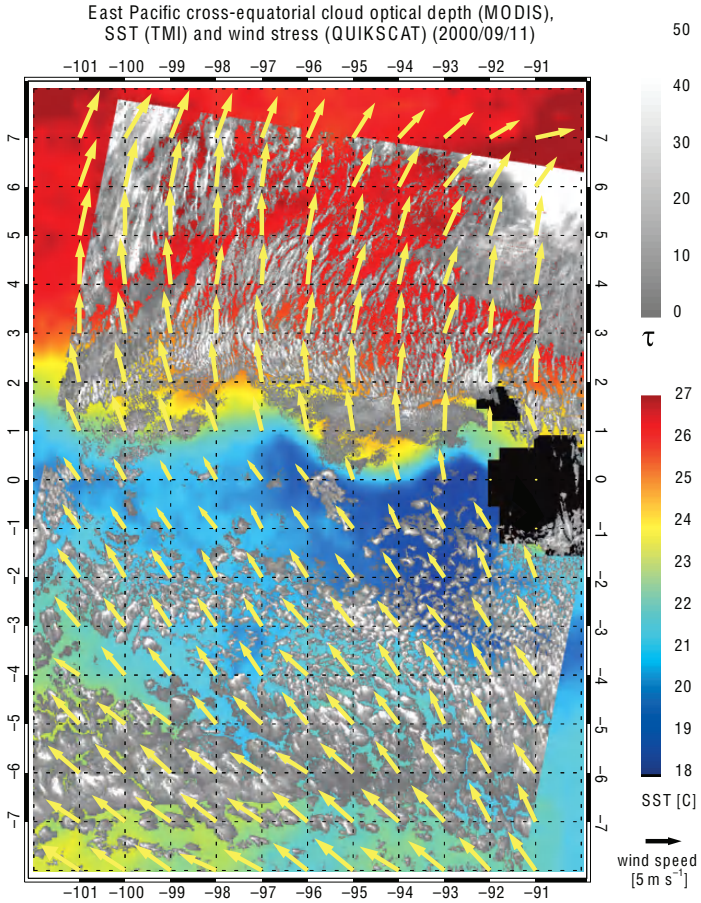

Fig. 9.40 Sea surface temperature (colored shading) surface winds (arrows) and clouds (gray shading) over the equatorial Pacific at a time when the equatorial front in the sea surface temperature field is well defined along 1 °N. The scalloped appearance of the front is due to the presence of tropical instability waves in the ocean. [Based on NASA QUIKSCAT, TMI, and MODIS imagery. Courtesy of Robert Wood.]

9.9 Prove that the definition of covariance reduces to the definition of variance for the covariance between any variable and itself.

9.10 Given the following variances in $m^2\ s^{-2}$

Where:	Location A		Location B	
When (UTC):	1000	1100	1000	1100
σ_u^2	0.50	0.50	0.70	0.50
σ_v^2	0.25	0.50	0.25	0.25
σ_w^2	0.70	0.50	0.70	0.25

When, where, and for which variables is the turbulence (a) stationary, (b) isotropic, and (c) homogeneous?
Some, but not all, of the answers Homogeneous for u wind at 1100 UTC. Stationary for v wind at location B. Isotropic at location A at 1100 UTC.

9.11 Given the following synchronous time series for T(°C) and w(m/s), find (a) mean temperature, (b) mean velocity, (c) temperature variance, (d) velocity variance, and (e) kinematic heat flux.

T	21	22	20	25	25	15	18	23	21	24	16	12	19	22
w	1	−2	0	−3	2	−2	−3	3	0	0	1	4	−2	−3

9.12 Under what conditions is the Richardson number not likely to be a reliable indicator for the existence of turbulence? Why?

9.13 If the dissipation length scale is L_ϵ, what is the e-folding time for the decay of turbulence (i.e., time for TKE/m to equal $1/e$ of its initial value), assuming you start with finite TKE but there is no production, consumption, transport, or advection?

9.14 The upward vertical heat flux in soil and rock due to molecular conduction is given by

$$F = -K\frac{\partial T}{\partial z} \tag{9.34}$$

where K is the *thermal conductivity* of the medium, in units of $W\ m^{-1}\ K^{-1}$, which ranges in value from 0.1 for peat to 2.5 for wet sand. From the first law of thermodynamics, we can write

$$C\frac{\partial T}{\partial t} = -\frac{\partial F}{\partial z} = \frac{\partial}{\partial z}K\frac{\partial T}{\partial z} \tag{9.35}$$

where C is the heat capacity per unit volume in $J\ m^{-3}\ K^{-1}$ (i.e., the product of the specific heat times the density). If K is assumed to be independent of depth

$$\frac{\partial T}{\partial t} = D\frac{\partial^2 T}{\partial z^2} \tag{9.36}$$

where $D = K/C$ is called the *thermal diffusivity*. Consider the response of the subsurface temperature to a sinusoidal variation in surface temperature with amplitude T_s and period P. (a) Show that the amplitude of the response drops off exponentially with depth below the surface with an e-folding depth of

$$h = \sqrt{\frac{DP}{2\pi}}$$

(b) The e-folding depth of the annual cycle, as estimated from Fig. 9.12, is ~2 m. Estimate the e-folding depth of the diurnal cycle at the same site.

9.15 For the situation shown in Fig. 9.12 in the text: (a) Making use of Eq. (9.36), derive a relationship for the phase lag Δt between the temperature wave at two depths differing by height Δz, given P the wave period and D the thermal diffusivity of the soil as defined in the previous exercise. (b) Using the annual cycle data given in Fig. 9.12 in the text, estimate the phase lag between the temperature curves at 1.5 and 6 m and then use it to find the value of D.

9.16 Given the heat-flux profile of Fig. 9.22, extend the method of Fig. 9.8 to estimate the sign of the triple correlation $\overline{w'w'\theta'}$ in the middle of the mixed layer, which is one of the unknowns in Eq. (9.11).

9.17 Given: $F_{HS} = 0.2\ K\ m\ s^{-1}$, $z_i = 1$ km, $u_* = 0.2\ m\ s^{-1}$, $T = 300$ K, $z_0 = 0.01$ m, find and explain the significance of the values of the (a) Deardorff velocity scale; (b) Obukhov length; (c) convective time scale; and (d) wind speed at $z = 30$ m.

9.18 The *flux form of the Richardson number* is

$$R_f = \frac{(g/\overline{T}_v)\,\overline{w'\theta'_v}}{\overline{w'u'}\dfrac{\partial \overline{u}}{\partial z} + \overline{w'v'}\dfrac{\partial \overline{v}}{\partial z}}$$

Use gradient transfer theory to show how R_f is related to R_i.

9.19 If the wind speed is 5 m s^{-1} at $z = 10$ m and the air temperature is 20 °C at $z = 2$ m, then (a) what is the value of the sensible heat flux at the surface of unirrigated grassland if the skin temperature is 40 °C? (b) What is the value of the latent heat flux? [**Hint**: $\rho c_p \approx 1231$ (W m^{-2})/(K m s^{-1}) for dry air at sea level.]

9.20 (a) Confirm that the following expression is a solution to Eq. (9.26), and (b) that it satisfies the boundary condition that $V = 0$ at $z = z_0$.

$$\frac{V}{u_*} = \frac{1}{k}\left\{\ln\frac{z}{z_0} - 2\ln\left[\frac{1+x}{2}\right] - \ln\left[\frac{1+x^2}{2}\right] + 2\arctan x - \pi/2\right\}$$

where

$$x = \left[1 - 15\frac{(z - z_0)}{L}\right]^{1/4}$$

9.21 Use the expressions for surface-layer wind speed from Eq. (9.22), from Exercise 9.4 in Section 9.3.3, and from the previous exercise to plot curves of V vs. z for (a) neutral ($L = \infty$), (b) stable ($L = 100$ m), and (c) unstable ($L = -10$ m) stratifications and confirm that their relative shapes are as plotted in Fig. 9.17a and 9.17b. Use $z_0 = 0.1$ m.

9.22 (a) If boundary-layer divergence is constant during fair weather, the mixed layer can stop growing during midafternoon even though there are strong sensible heat fluxes into the boundary layer at the ground. Why? (b) If w_e = constant, derive an equation showing the growth of z_i with time in a region where divergence β is constant.

9.23 If F^* is known, and if $|F_G| = 0.1 \cdot |F^*|$, then show how knowledge of time-averaged temperature at two heights in the surface layer and of mean humidity at the same two heights is sufficient to estimate the sensible and latent heat fluxes in the surface layer.

9.24 As a cold, continental air mass passes over the Gulf Stream on a winter day, the temperature of the air in the atmospheric boundary layer rises by 10 K over a distance of 300 km. Within this interval the average boundary layer depth is 1 km and the wind speed is 15 m s^{-1}. No condensation is taking place within the boundary layer and the radiative fluxes are negligible. Calculate the sensible heat flux from the sea surface.

9.25 (a) If drag at the ground represents a loss of momentum from the mean wind, determine the sign of $\overline{u'w'_s}$ if the mean wind is from the west. Justify your result.

(b) Do the same for a wind from the east, remembering that drag still represents a momentum loss.

9.26 Given the following temperature profile, determine and justify which layers of the atmosphere are (a) statically stable, (b) neutral, and (c) unstable.

z (km)	θ (°C)
2	21
1.8	23
1.6	19
1.4	19
1.2	13
1.0	16
0.2	16
0	10

9.27 If the total accumulated surface heat flux from sunrise through sunset is 5100 km, then use the sunrise sounding in the previous exercise to estimate the depth and potential temperature of the mixed layer just before sunset.

9.28 Given a smoke stack half the height of a valley: (a) describe the path of the centerline of the smoke plume during day and night during fair weather and (b) describe the centerline path of the smoke on a strongly windy day.

9.29 If you know the temperature and humidity jumps across the top of the mixed layer and if you know only the surface heat flux (but not the surface moisture flux), show how you can calculate the entrained heat and moisture fluxes at the top of the mixed layer.

9.30 Show that over flat terrain the large-scale vertical velocity at the top of the boundary layer is approximately equal to

$$w_i \simeq -z_i\{\nabla \cdot \mathrm{V}\} \tag{9.28}$$

where

$$\{\nabla \cdot \mathrm{V}\} \equiv \frac{\int_{p_i}^{p_s} (\nabla \cdot \mathrm{V})\, dp}{(p_s - p_i)}$$

is the mass-weighted divergence in the boundary layer and p_s and p_i are the pressures at the Earth's surface and at the top of the boundary layer.